An Energy Efficient Optimal Control Framework for General Purpose Flight Management Systems

Maxim Kaptsov

A Thesis

in

The Department

of

Electrical and Computer Engineering

Presented in Partial Fulfillment of the Requirements

for the Degree of

Master of Applied Science (Electrical and Computer Engineering) at

Concordia University

Montréal, Québec, Canada

July 2017

CONCORDIA UNIVERSITY

School of Graduate Studies

This is to certify that the thesis prepared

By: **Maxim Kaptsov**

Entitled: **An Energy Efficient Optimal Control Framework for General Purpose Flight Management Systems**

and submitted in partial fulfillment of the requirements for the degree of

Master of Applied Science (Electrical and Computer Engineering)

complies with the regulations of this University and meets the accepted standards with respect to originality and quality.

Signed by the Final Examining Committee:

_____ Chair
Dr. Rabin Raut

_____ External Examiner
Dr. Catharine Marsden

_____ Examiner
Dr. Akshay Kumar Rathore

_____ Supervisor
Dr. Luis Rodrigues

Approved by _____
William E. Lynch, Chair
Department of Electrical and Computer Engineering

_____ 2017

_____
Amir Asif, Dean
Faculty of Engineering and Computer Science

Abstract

An Energy Efficient Optimal Control Framework for General Purpose Flight Management Systems

Maxim Kaptsov

Global warming has become one of the biggest environmental issues. To reduce its effect on climate change, the aviation industry is constantly looking for ways to decrease fuel emissions of modern airplanes, either by applying new technologies to existing airplane structures or by increasing the aircraft performance in flight. These measures could reduce significantly the fuel consumption of today's commercial airplanes. Among other solutions proposed by various engineers, the use of renewable energy sources looks especially promising since electric engines could provide near emission-free propulsion.

This thesis proposes an optimal control framework for flight management systems of turbofan and all-electric aircraft. The optimal control problem of economy mode is solved using Pontryagin's minimum principle. The economy mode optimization problem corresponds to the minimization of a functional parameterized by a coefficient index that performs a trade-off between the cost of fuel or battery charge and time-related costs. For the turbofan, a sub-optimal numerical solution for the true airspeed of an aircraft flying at cruise altitude is obtained. The speed can be easily computed using fast-converging algorithms such as Newton's method. For all-electric aircraft, an optimal algebraic solution for the true airspeed during the cruise segment is obtained. Additionally, the maximum endurance and the maximum range are obtained as analytical expressions of the parameters.

Overall, the developments presented in this thesis provide a method to obtain the optimal speed schedules for on-board flight management systems of commercial airplanes and also extend the theory of aircraft performance to the case of electric airplanes.

Acknowledgments

I would first like to thank my thesis advisor Dr. Luis Rodrigues for the continuous support of my MASc study and related research, for his patience, motivation, and immense knowledge. The door to Prof. Rodrigues' office was always open whenever I ran into a trouble spot or had a question about my research or writing. He consistently steered me in the right the direction whenever he thought I needed it.

I thank my fellow labmates: Michael, Alex, Amir, Julia, Emily, Mailis, and Bruno. Thank you for the stimulating discussions and for all the fun we have had in the last couple of years.

I would like also to extend my gratitude to Mitacs and TRU Simulation + Training for providing financial support, and for giving me the opportunity to obtain much-valued work experience as an intern by applying the results of my work in a practical environment.

Last but not least, I must express my very profound gratitude to my parents, my brother and to my beloved wife, Natalia, for providing me with unfailing support and continuous encouragement throughout my years of study and through the process of researching and writing this thesis. This accomplishment would not have been possible without them.

Contents

List of Figures viii

List of Tables ix

List of Symbols x

1 Introduction 1

1.1 Motivation . . . 1

1.2 Flight Management Systems . . . 2

1.3 Economy Mode . . . 3

1.4 Literature Survey . . . 3

1.5 Objectives . . . 4

1.6 Methodology . . . 5

1.7 Contributions . . . 5

1.8 Structure of the Thesis . . . 6

2 Theoretical Preliminaries 7

2.1 Aircraft Performance . . . 7

2.1.1 Aerodynamic Forces in Flight . . . 7

2.1.2 Longitudinal Flight Dynamics . . . 8

2.1.3 Specific Fuel Consumption . . . 9

2.2 Energy Conversion and Battery Models . . . 10

2.2.1 Energy Conversion . . . 10

2.2.2 Ideal Battery . . . 11
2.2.3 Battery with Internal Resistance . . . 11
2.3 Optimal Control . . . 13
2.3.1 Optimal Control Problem Formulation . . . 13
2.3.2 Maximum Principle for the Fixed-Endpoint Control Problem . . . 16
2.4 Quartic and Quintic Equations . . . 17
2.5 Descartes' Rule of Signs . . . 19
2.6 Shooting Method . . . 19

3 Economy Mode for Turbofan Aircraft 21
3.1 Introduction . . . 21
3.2 Assumptions . . . 22
3.3 Economy Mode Optimal Control Problem . . . 23
3.4 Suboptimal Solution of Economy Mode Optimal Control Problem . . . 26
3.5 Shooting Method . . . 27
3.6 Simulations . . . 27
3.6.1 Aircraft Model and Initial and Final Conditions . . . 27
3.6.2 Simulation Results . . . 28

4 Economy Mode and Maximum Endurance Optimal Solutions for All-Electric Aircraft 33
4.1 Introduction . . . 33
4.2 Assumptions . . . 34
4.3 Economy Mode Optimal Control Problem . . . 35
4.4 Maximum Endurance Optimal Control Problem . . . 46
4.5 Simulations . . . 51
4.5.1 Aircraft Model and Initial and Final Conditions . . . 51
4.5.2 Simulation Results . . . 52

5 Conclusions and Future Work 57
5.1 Conclusions . . . 57

5.2 Extensions 57

Bibliography **59**

List of Figures

Figure 2.1 Aerodynamic forces in level flight. 8

Figure 2.2 Constant current discharge curve of a typical Li-ion battery. 12

Figure 2.3 Geometric interpretation of an optimal control problem. 15

Figure 3.1 Specific fuel consumption as a function of true airspeed. 29

Figure 3.2 A close-up view of a section of the Fig. 3.1. 30

Figure 3.3 $J_W g$ as a function of the horizontal position. 30

Figure 3.4 True airspeed as a function of the aircraft weight for $C_I = 0$. 31

Figure 3.5 Weight as a function of the horizontal position for $C_I = 0$. 31

Figure 3.6 True airspeed as a function of the aircraft weight for different C_I. 32

Figure 3.7 Weight as a function of the horizontal position for different C_I. 32

Figure 4.1 E-Fan technology demonstrator. 52

Figure 4.2 E-Fan cross-Channel flight route. 54

Figure 4.3 Comparison of velocities obtained for different battery models. 55

Figure 4.4 Pareto-optimal trade-off curve. 56

List of Tables

Table 3.1 Boeing 737-800 technical data 28
Table 3.2 Simulation initial and final conditions 28
Table 4.1 E-Fan 1.0 technical data 53
Table 4.2 Simulation initial and final conditions 53

List of Symbols

$Æ$	Aspect ratio
c	Speed of sound, m/s
C_D	Drag coefficient
$C_{D,0}$	Zero-lift drag coefficient
C_I	Cost index, kg/s or A
C_I^{crit}	Critical cost index, A
C_L	Lift coefficient
C_t	Time-related costs, $\$/s$
C_q	Cost of the battery charge, $\$/C$
D	Drag, N
e	Span efficiency factor
f	Fuel flow mass rate, kg/s
g	Gravitational acceleration, m/s^2
E	Maximum endurance, s
H	Hamiltonian, kg/s or A
h	Altitude, m
i	Battery current, A
J	Total flight cost, kg or C
J_Q	Partial derivative of the cost J with respect to the variable Q, $1/A$
J_W	Partial derivative of the cost J with respect to the variable W, s^2/m
J_x	Partial derivative of the cost J with respect to the variable x, kg/m or C/m

K	Induced drag constant
L	Lift, N
M_∞	Free-stream Mach number
P_e	Electric power, W
Q	Battery charge, C
R	Maximum range, m
S	Wing area, m^2
S_{FC}	Thrust specific fuel consumption, $kg/(N \cdot s)$
t	Time, s
T	Thrust, N
T°_{FL}	Ambient temperature at the flight altitude, K
T°_{SL}	Standard temperature at sea level, K
U	Battery voltage, V
v	True airspeed, m/s
v_{crit}	Critical velocity, m/s
W	Weight, N
x	Horizontal position, m
α	Angle of attack, rad
γ	Flight path angle, rad
η	Overall system efficiency
ρ	Air density, kg/m^3

Chapter 1

Introduction

1.1 Motivation

There are several reasons to study aircraft performance and apply flight trajectory optimization techniques. Today the aviation produces approximately 780 million tonnes of carbon dioxide (CO_2) annually, which constitutes 12 % of CO_2 emissions from all transport sources [1]. An inevitable growth of air traffic (which is estimated to almost triple by 2035 [2]) implies the consequent increase of the amount of fuel burned and an even heavier impact on the environment. Hence, the industry's efforts to reduce harmful emissions are of utmost importance. On the other hand, the airlines should be invested in reducing fuel consumption since that could help maximize their revenue.

Along with optimizing the flight performance of kerosene-fueled airplanes, the leading aircraft manufacturers turned their attention to the development of electric-powered aerial vehicles. Recent years have marked a significant step forward in this direction. With the aid of modern lithium-ion batteries, all-electric powered flight has already become possible for light aircraft. For example, the Airbus E-Fan [3] prototype flew across the English Channel in 2015 and NASA is working on a battery-powered research plane X-57 [4] scheduled for a test flight in 2017.

Due to the rather limited mass specific energy of the batteries (compared to fossil fuels), it is unlikely that an electric aircraft could compete with long range passenger jets in the foreseeable future [5]. However, on the short haul routes, a hybrid electric airplane may be able to challenge regional jets and turboprops by cutting significantly fuel costs while an all-electric aircraft could

prove invaluable for recreational and/or training flights.

In commercial aircraft, the task of optimizing its trajectory is performed by the on-board flight management system (FMS) computer. It is natural to assume that at some point an electric aircraft will require a similar system.

1.2 Flight Management Systems

Essentially, the FMS is a specialized navigation, flight planning, and performance computer. It provides airspeed, altitude, climb and descent points corresponding to the most economical fuel consumption. In doing so, the system uses flight paths stored in its database, but also allows the pilot to modify them and select various flight control modes via the multifunction control display unit (MCDU). The FMS generates and displays flight path profile, navigation and performance data. It also issues commands to the autopilot. Additionally, it provides continuous automatic navigation from the moment of take-off until landing. All in all, its functions can be summarized as follows:

- obtain the best estimate of the current aircraft state;
- provide aircraft performance information;
- determine flight routes for the aircraft;
- predict the trajectory along the specified flight route (profile);
- guide aircraft along the computed profile;
- derive the optimal speed and altitude based on accumulated performance data.

The FMS is installed on board of most modern commercial and business airplanes. It was first designed for the Boeing 757 and 767 in the early 1980s, although simpler systems existed earlier [6].

1.3 Economy Mode

Generally, in order to achieve energy-efficient flights, the aircraft operators seek to minimize the Direct Operating Cost (DOC) given by the following expression

$$DOC = C_f \Delta f + C_t \Delta t$$

where C_f is the cost of fuel per unit of mass, Δf is the total mass of fuel burned, C_t is the cost of flight per unit of time representing time-related costs such as crew salary or maintenance costs, and Δt is the trip time. Assuming that C_f is constant for the duration of flight, the problem of minimizing the DOC is equivalent to minimizing

$$DOC^* = \Delta f + C_I \Delta t$$

where C_I is the so-called cost index. The importance of C_I is that the Economy Mode (ECON) in an FMS uses it to make a trade-off between fuel burned and trip time. Essentially, speed schedules for optimal operation of the aircraft in the climb, cruise and descent phases of flight are determined as a function of C_I, so that for any value of C_I chosen by the operator, the FMS computer can obtain the most economical speed.

A similar approach can be applied to electric aircraft where the battery charge is considered in place of fuel.

1.4 Literature Survey

Aircraft trajectory optimization has been a topic of research for at least 50 years. Miele [7] conducted a comprehensive survey of the flight path optimization problems for fuel propelled aircraft in the 1960s. Some of the earlier algorithms for the conventional fuel-powered aircraft DOC trajectory optimization based on energy state methods can be found in [8, 9]. Aircraft trajectory optimization at constant altitude was studied in [10]. The related subject of fuel- and time-efficient flights have also been discussed extensively by many authors. For example, in [11], the authors addressed the

problem of minimum-cost cruise in the presence of winds. A flight trajectory optimization method using genetic algorithms to minimize fuel consumption for the lateral and vertical navigation modes was proposed in [12]. More recently, in [13], the authors obtained an analytical solution to the optimal velocity of a turbojet airplane cruising at fixed altitude.

There has been also a significant effort in the literature to address battery-powered airplanes. This effort is occurring in parallel with recent contributions on nonlinear modeling of lithium-ion (Li-ion) batteries. Ref. [14] proposed a model for the open voltage source as a function of the actual State of Charge (SOC) of the battery. Energy management and performance optimization of unmanned aerial vehicles (UAV) based on optimal control techniques can be found in [15, 16, 17]. Hepperle [5] studied limitations imposed on design of electric airplanes by modern batteries and obtained an expression for the maximum range as a function of battery parameters. He subsequently proposed several aircraft designs optimized for electric propulsion. However, the aircraft velocity optimization was not studied in his work. Traub [18] obtained expressions to estimate the maximum range and endurance (as well as the required flight velocities) of a battery-powered aircraft. However, optimal control methods were not employed and consequently a trade-off between the cost of battery charge and time-related costs was not incorporated into the solution. Recently, Donateo at al. [19] calculated the net endurance of hybrid electric aircraft and compared it to the gross endurance. In [20], the authors conducted a multidisciplinary design optimization to design a hybrid electric aircraft powertrain.

1.5 Objectives

To the best of the author's knowledge, there are no optimal solutions of trajectory optimization of a turbofan and all-electric aircraft in the open literature. In most cases, the turbofan model is simplified to that of a turbojet, allowing for a closed form solution at the expense of accuracy. Electric airplanes, a relatively new direction in aerospace engineering, have not attracted as much attention as their fuel-powered counterparts have, and therefore have not benefited yet from the trajectory optimization and the trade-off analysis between time-related costs and energy cost.

The objective of this thesis is to obtain optimal true airspeeds that generate cost-optimal trajectories for the cruise flight segment in terms of the cost index. Suboptimal solutions are acceptable, provided that they are adequately close to the optimal and suitable for implementation in a real FMS. The maximum range and maximum endurance of an all-electric aircraft are also considered.

1.6 Methodology

The ECON mode (both turbofan and all-electric aircraft) and the maximum endurance (all-electric aircraft only) will be formulated as optimal control problems (OCP) for the cruise segment. The model of an aircraft flying in the longitudinal plane will be considered in the state-space representation, and some assumptions will be used to simplify it. To solve the OCP, Pontryagin's Minimum Principle (PMP) will be employed. To validate the obtained optimal solutions for turbofan aircraft, the Two-Point Boundary Value Problem (2PBVP) will be solved using a shooting method. Optimal solutions for all-electric aircraft will be compared against available experimental data for existing electric aircraft. Boeing 737-800 and Airbus E-Fan 1.0 model are used to perform simulations.

1.7 Contributions

This thesis contributes to the area of flight management systems. Specifically, the following results are obtained considering the cruise flight segment:

- For turbofan aircraft, a suboptimal speed is obtained as a root of the 5^{th} degree polynomial whose coefficients are fixed and/or contain known states. The root can be easily computed by means of a fast-converging algorithm such as Newton's method.

- For all-electric aircraft, both analytical and numerical optimal solutions for the true airspeed, maximum range, and maximum endurance are found using Pontryagin's minimum principle. The analytical solution is applicable for the ideal battery models whereas the numerical solution is required when considering batteries with internal resistance. To the best of the author's knowledge, this is the first time that such solutions are proposed.

1.8 Structure of the Thesis

Chapter 2 lays down the theoretical basis needed for understanding the rest of the thesis. This is followed by Chapter 3, which derives the economy mode results for turbofan aircraft. A sub-optimal numerical solution for the optimal speed is obtained, which is compared to the solution obtained by the shooting method at the end of the chapter. Next, Chapter 4 applies the same methods to all-electric aircraft. The economy mode and maximum range optimal control problems are solved analytically. Additionally, the maximum endurance of all-electric aircraft is studied. Lastly, Chapter 5 draws the main conclusions of this thesis and provides extensions for future work.

Chapter 2

Theoretical Preliminaries

2.1 Aircraft Performance

Airplane performance is the subject of this Section. First, the forces in flight – lift, drag, thrust, and weight – are reviewed. Then, a dynamic model of an aicraft is presented. The Section terminates with a brief discussion of specific fuel consumption.

2.1.1 Aerodynamic Forces in Flight

This subsection brifly describes aerodynamic forces acting on an airplane in level flight (see Fig. 2.1). Drag is a force exerted on an aircraft moving through air and it is oriented in the direction of relative air flow. To cruise at a steady speed in a horizontal direction, an aircraft must generate enough thrust to overcome the drag force. Thrust can be produced by spinning a propeller or by high-speed jet exhaust or a combination of both. A flying aircraft also generates a lift force which is directed perpendicular to the drag force, opposing the weight of the aircraft.

Lift and drag forces that act on an aircraft in flight are given by the following equations [21]:

$$L = \frac{1}{2} C_L \rho S v^2, \tag{1a}$$

$$D = \frac{1}{2} C_D \rho S v^2 \tag{1b}$$

where C_L and C_D are lift and drag coefficients, respectively, ρ is the air density, S is the wing area,

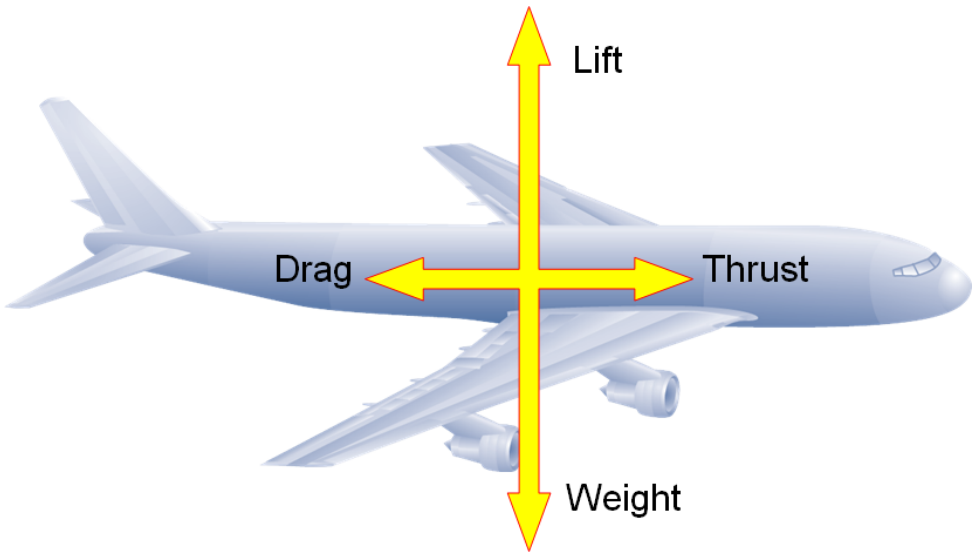

Figure 2.1: Aerodynamic forces in level flight.

and v is the velocity.

An equation for steady flight drag force D was developed in [13, 21] for flight below drag divergence Mach number and is given by

$$D = \frac{1}{2} C_{D,0} \rho S v^2 + \frac{2KW^2}{\rho S v^2} \tag{2}$$

where $C_{D,0}$ is the zero-lift drag coefficient, K is the induced drag constant and W is the weight.

2.1.2 Longitudinal Flight Dynamics

The nonlinear longitudinal dynamic model of an aircraft is given by the following differential equations [13, 21]

$$
\begin{aligned}
\dot{x} &= v\cos\gamma \\
\dot{h} &= v\sin\gamma \\
\dot{v} &= \left(\frac{g}{W}\right)(T\cos\alpha - D - W\sin\gamma) \\
\dot{\gamma} &= \left(\frac{g}{Wv}\right)(T\sin\alpha + L - W\cos\gamma) \\
\dot{W} &= -S_{FC}Tg
\end{aligned}
\tag{3}
$$

where x is the horizontal position, h is the altitude, v is the velocity, γ is the flight path angle, α is the angle of attack, T is the thrust, S_{FC} is the specific fuel consumption, and g is the gravitational acceleration.

2.1.3 Specific Fuel Consumption

Specific fuel consumption S_{FC} describes the fuel efficiency of an engine, i.e. how efficiently it burns fuel and converts it into power. For turbojet and turbofan aircraft S_{FC} can be thought of as the mass of fuel used per unit of time per unit of thrust:

$$
S_{FC} = \frac{\Delta W_{fuel}}{\Delta t \cdot Tg} \tag{4}
$$

where ΔW_{fuel} is the weight of fuel used. Alternatively, (4) can be written in the differential form

$$
S_{FC} = -\frac{\dot{W}}{Tg} = \frac{f}{T} \tag{5}
$$

where f is the fuel mass flow rate. Specific fuel consumption varies with with speed and altitude, although it is usually assumed that S_{FC} is constant with altitude. For turbofan aicraft the variation of S_{FC} with velocity can be described as [21, 22]

$$
S_{FC} = A^*(1 + BM_\infty)\sqrt{T^\circ_{FL}/T^\circ_{SL}} \tag{6}
$$

where A^* and B are empirical constants that vary from one engine to another, M_∞ is the Mach number, T°_{FL} is the ambient temperature at the flight altitude, and $T^\circ_{SL} = 288.2K$ is the standard temperature at sea level. Equation (6) only holds for a limited range $0.7 < M_\infty < 0.85$ corresponding to cruise Mach numbers.

2.2 Energy Conversion and Battery Models

With a jet engine, the only transformation step is the conversion of chemical energy in fuel to kinetic energy, and the specific fuel consumption, covered in the previous section, is a figure of merit of such transformation. In this Section, we briefly discuss energy transformations in electric aicraft and consider relevant battery models.

2.2.1 Energy Conversion

Electric airplanes being developed by major aerospace companies are powered by either batteries or a hybrid electric system, featuring also a small combustion engine within the fuselage to provide an extended range or endurance. Electrical energy stored in a battery in the form of chemical energy usually chemical energy, is transformed into electricity; and then it is transformed into the kinetic energy of motion. The thrust is usually generated by a combination of propellers (e.g., ducted fans). For the aircraft in cruise at velocity v the net power required is [21]

$$P_R = Tv = \eta P_e \tag{7}$$

where η is the overall system efficiency. In turn, the electric power P_e produced by the electric current i is given by

$$P_e = Ui = -U\dot{Q} \tag{8}$$

where Q is the battery charge. Note the minus sign in front of the voltage U which indicates that the positive direction is defined as the current being drawn from the battery (i.e., the aircraft must consume the battery charge during flight).

2.2.2 Ideal Battery

To obtain an elegant analytical solution for the optimal speed, we first consider the model of an ideal voltage source based on the characteristics depicted in Fig. 2.2, which shows a typical discharge curve for Li-ion batteries. The following assumptions are made regarding the battery model:

1. The internal resistance is small and can be neglected by replacing its effects by a slight reduction in the efficiency factor η.

2. The battery's output voltage does not vary much with the state of charge (SOC). More specifically it is assumed that (see Fig. 2.2): a) the exponential discharge occurs in a relatively small time interval and can be neglected; b) charge corresponding to the knee portion of the curve after the nominal zone of constant voltage will be left as a safety reserve and will be considered only for the maximum range and maximum endurance.

3. The electromotive force is independent of the battery's temperature.

4. The battery capacity does not depend on the amplitude of the current (no Peukert effect [23]).

Under assumptions 1–4, the output voltage is constant and the battery model is

$$U = U_{nom} \tag{9}$$

where U_{nom} is the nomimal battery voltage corresponding to the nominal zone (see Fig. 2.2).

Solving (7)–(8) for $\dot{Q}$ yields another state equation required to describe the model

$$\dot{Q} = -i = -\frac{Tv}{\eta U}. \tag{10}$$

2.2.3 Battery with Internal Resistance

Using the battery model with internal resistance allows one to obtain a more accurate solution for the optimal speed. However, it will be shown later that an analytical solution for the ECON mode is no longer attainable. The following assumptions are made regarding the battery model:

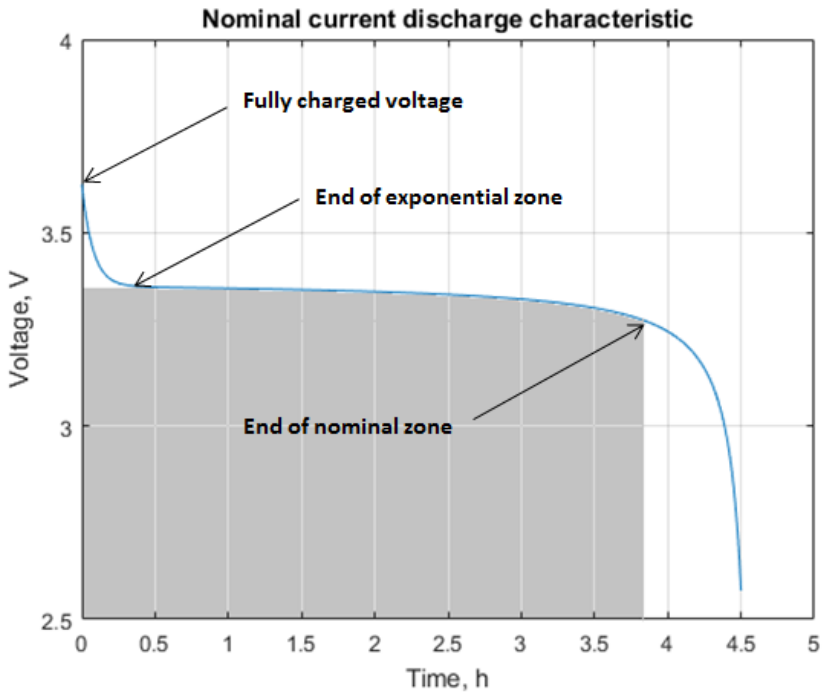

Figure 2.2: Constant current discharge curve of a typical Li-ion battery.

1. The battery output voltage U does not vary much with the state of charge.

2. The electromotive force is independent of the battery's temperature.

3. The battery capacity does not depend on the current amplitude.

4. The internal resistance r does not change with cycling and age.

Under assumptions 1–4, the battery output voltage is

$$U = U_{nom} - ir. \tag{11}$$

Combining (7)–(8) and (11) yields a quadratic equation in i

$$\eta r i^2 - \eta U_{nom} i + Tv = 0, \tag{12}$$

whose solutions are

$$i = \frac{U_{nom}}{2r} \pm \frac{\sqrt{(\eta U_{nom})^2 - 4\eta r T v}}{2\eta r}. \tag{13}$$

While both solutions (13) yield feasible results, from an engineering point of view it is preferable to have a combination of higher output voltage and lower electric current to limit the effect of power dissipation due to the internal resistance. Therefore, an equation for the electric current as an explicit function of T and v is

$$i = -\dot{Q} = \frac{U_{nom}}{2r} - \frac{\sqrt{(\eta U_{nom})^2 - 4\eta r T v}}{2\eta r}. \tag{14}$$

There are, of course, more sophisticated state-dependent battery models in the open literature. In [14], the authors developed a model for the open voltage source as a function of the SOC of the battery and proposed a method to extract the dynamic model parameters from batteries datasheets. However, using complex algorithms would certainly hinder the implementation.

2.3 Optimal Control

Optimal control theory is concerned with finding optimal inputs to control a dynamic system based on a given performanse measure. The two main methods to solve optimal control problems are dynamic programming based on Bellman's principle of optimality and the maximum principle, which originated from calculus of variations. The latter approach is used in this thesis. The maximum (or minimum) principle was formulated by Lev Pontryagin and his associates in 1956, and since then bears his name. This section provides a quick review of the Pontryagin's maximum principle (PMP) based on [24].

2.3.1 Optimal Control Problem Formulation

The following optimal control problem is formulated assuming that

1) the control system and the running cost do not depend on time;

2) the endpoint is fixed while the final time is not;

3) there is no terminal cost.

Among all admissible controls $u = u(t)$, taking a dynamical system from the state x_0 to the state x_f, we need to find u that minimizes the functional

$$J = \int_{t_0}^{t_f} f^0(x(t), u(t))dt = \int_{t_0}^{t_f} L(x(t), u(t))dt \tag{15}$$

where the initial time t_0 is known and the final time t_f is unspecified. The control system can be described by the state equation

$$\frac{dx}{dt} = f(x, u) \tag{16}$$

where $x = (x^1, x^2, ...x^n)$ is the state vector, $i = 1, 2...n$. Another state is added to the states x, namely x^0, such that

$$\frac{dx^0}{dt} = L(x, u) \tag{17}$$

where L is the function which is used to define the functional J. In other words, the set of ODEs is considered as

$$\frac{dx^i}{dt} = f^i(x^1, x^2..., x^n, u) \equiv f^i(x, u) \tag{18}$$

where the right-hand side does not depend on x^0 and $i = 0, 1, 2...n$. Letting $\tilde{x} = (x^0, x^1, ..., x^n) = (x^0, x)$, (18) can be rewritten as

$$\frac{d\tilde{x}}{dt} = \tilde{f}(x, u) \tag{19}$$

where $\tilde{f}(x, u)$ is the vector in the space $\tilde{X}$ whose coordinates are $f^0(x, u), ..., f^n(x, u)$.

Let $u(t)$ be a admissible control input taking a dynamical system from the initial state x_0 to the final state x_f and $x(t)$ be a corresponding solution of equation (16) with the initial condition $x(t_0) = x_0$. Let $\tilde{x_0}$ be the point $(0, x_0)$, i.e. a point in the space $\tilde{X}$ with coordinates $0, x_0^1, ..., x_0^n$, where $x_0^1, ..., x_0^n$ are the coordinates of point x_0 in space X. Then the solution of equation (19), corresponding to the control $u(t)$, with the initial condition $\tilde{x}(t_0) = \tilde{x}_0$ is defined for all $t_0 \leq t \leq t_f$ and has the form

$$\begin{aligned} x^0 &= \int_{t_0}^{t} f^0(x(t), u(t))dt \\ x &= x(t) \end{aligned} \tag{20}$$

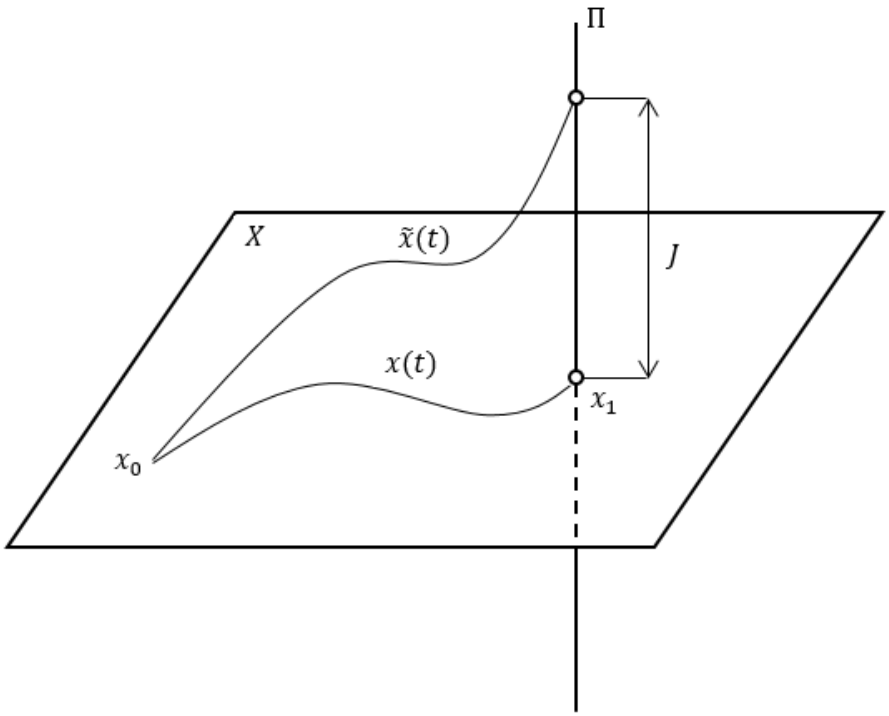

Figure 2.3: Geometric interpretation of an optimal control problem.

In particular, at $t = t_f$ (20) becomes

$$\begin{aligned} x^0 &= \int_{t_0}^{t_f} f^0(x(t), u(t))dt = J \\ x &= x_f \end{aligned} \tag{21}$$

i.e. the solution $\tilde{x}(t)$ of equation (19) with the initial condition $\tilde{x}(t_0) = \tilde{x}_0$ passes through the point $\tilde{x} = (J, x_f)$. In other words, by defining a line Π (see Fig. 2.3) in the space $\tilde{X}$, passing through the point $\tilde{x} = (0, x_f)$ parallel to the axis x^0, one can say that the solution $\tilde{x}(t)$ passes through the point $x^0 = J$ on the line Π at time $t = t_f$. The minimum possible value of the coordinate x^0 corresponds to the optimal cost J^*.

The maximum principle for this particular problem is formulated in the following subsection.

2.3.2 Maximum Principle for the Fixed-Endpoint Control Problem

The following theorem was formulated in [24]. An equivalent, modern formulation can be found in [25].

Theorem 1. *Let $u(t)$, $t_0 \leq t \leq t_f$, be an admissible control input such that the corresponding state trajectory $x(t)$, starting from point x_0 at time t_0, passes through a point x_f at time t_f (see Fig. 2.3). For $u^*(t)$ and $x^*(t)$ to be optimal it is necessary that there exists a non-zero continuous vector function $\lambda(t)$ and a constant $\lambda_0^*(t) \leq 0$, corresponding to the functions $u(t)$ and $x(t)$, such that:*

1) $\lambda(t)$ and $x(t)$ satisfy the following Hamiltonian system

$$\begin{aligned} \frac{dx}{dt} &= \frac{\partial H}{\partial \lambda} \\ \frac{d\lambda}{dt} &= -\frac{\partial H}{\partial x} \end{aligned} \tag{22}$$

where the Hamiltonian H is defined as

$$H = \lambda^T f(x,u) + \lambda_0 L(x,u).$$

2) For any t, $t_0 \leq t \leq t_f$, the function $H(x(t), u, \lambda(t))$ of variable $u \subset U$ reaches its maximum at point $u = u^*(t)$

$$H(x^*(t), u^*(t), \lambda^*(t), \lambda_0^*) \geq H(x^*(t), u(t), \lambda^*(t), \lambda_0^*) \tag{23}$$

3) For any t, $t_0 \leq t \leq t_f$, the following holds

$$H(x^*(t), u^*(t), \lambda^*(t), \lambda_0^*) = 0. \tag{24}$$

As we shall see in the chapters to follow, PMP provides an effective tool to solve optimal control problems pertaining to aircraft trajectory optimization.

2.4 Quartic and Quintic Equations

The methods developed in the present thesis require solving equations of the 4^{th} (*quartics*) and 5^{th} (*quintics*) order. An efficient method for obtaining roots of general quartic equations can be found in [26]. Without loss of generality, consider the quartic equation

$$x^4 + a_3x^3 + a_2x^2 + a_1x + a_0 = 0. \tag{25}$$

Equation (25) can be reduced to the depressed form

$$y^4 + y^3 + py^2 + qy + r = 0 \tag{26}$$

using a substitution

$$y = x - \frac{a_3}{4}$$

where

$$\begin{aligned} p &= a_2 - \frac{3a_3^2}{8} \\ q &= \frac{a_1^3}{8} - \frac{a_1a_2}{2} + a_0. \end{aligned} \tag{27}$$

If the associated resolvent cubic equation

$$z^3 - a_2z^2 + (a_3a_1 - 4a_0)z + (4a_2a_0 - a_1^2 - a_3^2a_0) = 0 \tag{28}$$

has a real root, then the quartic (26) can be factorized. The general formula for one of the roots of (28) is

$$z = -\frac{1}{3}\left(-a_2 + Q + \frac{\Delta_0}{Q}\right) \tag{29}$$

where

$$
\begin{aligned}
Q &= \sqrt[3]{\frac{\Delta_1 + \sqrt{\Delta_1^2 - 4\Delta_0^2}}{2}} \\
\Delta_0 &= a_2^2 - 3(a_3 a_1 - 4a_0) \\
\Delta_1 &= 2a_2^3 + 9a_2(a_3 a_1 - 4a_0) + 27(4a_2 a_0 - a_1^2 - a_3^2 a_0).
\end{aligned}
\tag{30}
$$

Then the four roots of the general quartic (25) are

$$
\begin{aligned}
x_{1,2} &= -\frac{a_3}{4} - S \pm \frac{1}{2}\sqrt{-4S^2 - 2p + \frac{q}{S}} \\
x_{3,4} &= -\frac{a_3}{4} + S \pm \frac{1}{2}\sqrt{-4S^2 - 2p - \frac{q}{S}}
\end{aligned}
\tag{31}
$$

where

$$
S = \frac{1}{2}\sqrt{a_2 - \frac{1}{4}a_3^2 - z}.
$$

For more details see [27].

General quintic equations, on the other hand, do not have an algebraic solution, i.e. a solution in terms of a finite number of additions, subtractions, multiplications, divisions, and root extractions. This is known as the Abel–Ruffini theorem [28] which applies to the general polynomial equations of degree 5 and higher. However, there exist several approaches to solve a general quintic equation of the form

$$
x^5 + a_4 x^4 + a_3 x^3 + a_2 x^2 + a_1 x + a_0 = 0. \tag{32}
$$

First, the quintic is reduced to the so-called principal form where quartic and cubic terms are set to zero as:

$$
y^5 + b_2 y^2 + b_1 y + b_0 = 0 \tag{33}
$$

This is done by means of a quadratic transformation first proposed by the German mathematician Tschirnhaus in the XVII century. One of the approaches involves further reducing the quintic (33) to the so-called Bring-Jerrard form

$$
z^5 + c_1 z + c_0 = 0. \tag{34}
$$

The closed form solutions of the (34) can be expressed in terms of the hypergeometric functions in one variable, ${}_4F_3$, or, alternatively, in terms of the Bring radical BR

$$\sqrt[4]{-\frac{c_1}{5}}BR\left(-\frac{1}{4}\left(-\frac{5}{c_1}\right)^{\frac{5}{4}}c_0\right)$$

and its complex conjugates. Although these solutions are analytical, they are by no means algebraic. In fact, these solutions are too unwieldy to handle and implement in real-time systems since a substantial amount of time is required to obtain them. Therefore, a more convenient numerical approach will be used to solve 5^{th} order polynomial equations.

2.5 Descartes' Rule of Signs

Throughout this thesis, there are a number of instances where it is required to prove that a given quartic or quintic equation has a unique solution or to determine the number of positive or negative solutions. The rule of signs, first described by the famous French mathematician René Descartes, is a method for determining an upper bound on the number of positive and negative real roots of a polynomial.

Theorem 2. *In any polynomial in one variable with real coefficients (ordered by descending variable exponent) the number of positive roots of the polynomial is either equal to the number of change in sign between consecutive nonzero coefficients, or is less than it by an even number.*

The rule has a corollary stating that the number of negative roots is the number of sign changes after multiplying the coefficients of odd-power terms by 1, or is less than it by a multiple of 2.

2.6 Shooting Method

The shooting method is a method for solving a two-point boundary value problem (2PBVP) by reducing it to an initial value problem. Since 2PBVPs can have more than one solution, the method requires providing a sufficiently good guess for the desired solution (which is oftentimes the most difficult part of solving a 2PBVP). Essentially, a boundary value problem consists of a set of ODEs,

boundary conditions, and an initial guess. For a boundary value problem of a second-order ODE, the method can be described as follows [1]. Let

$$x'' = f(t, x(t), x'(t)), \qquad x(t_0) = x_0, \qquad x(t_1) = x_1$$

be the 2PBVP and $x(t_1; p)$ be the solution of the initial value problem

$$x'' = f(t, x(t), x'(t)), \qquad x(t_0) = x_0, \qquad x'(t_0) = p.$$

If $x(t_1; p) = x_1$, then the solution of the initial value problem is a desired solution of the 2PBVP. The solutions obtained using the shooting method can be considered optimal. MATLAB offers a `bvp4c` function to solve boundary value problems for ordinary differential equations. One must provide functions that evaluate the differential equations and the residual in the boundary conditions.

[1] https://en.wikipedia.org/wiki/Shooting_method

Chapter 3

Economy Mode for Turbofan Aircraft

3.1 Introduction

Minimizing aircraft operating costs is important from both financial and environmental points of view. Methods to decrease the operating costs can be applied to three broad areas:

- flight operations;
- air traffic control;
- technical maintenance.

Methods to improve flight operations include increasing the aircraft performance in flight and thorough preflight preparation, such as choosing the most advantageous route based on the predicted meteorological conditions or determining the optimal amount of fuel during the refueling process.

Air traffic control can be improved in terms of air traffic planning.

Finally, maintenance of the aircraft skin paint, power plants, and on-board system also contributes to decreasing the operating costs.

In the following sections, we propose a method to increase the aircraft performance in level flight and compute the most economical cruising speed.

3.2 Assumptions

The following assumptions will be used to simplify the model (3):

1. The aircraft is in steady flight at constant altitude, making $\gamma = \dot{\gamma} = \dot{h} = 0$.
2. The angle of attack α is small, therefore, $\cos\alpha \approx 1, \sin\alpha \approx \alpha$.
3. The altitude, thrust, and speed of the aircraft are within the flight envelope.
4. The component of the thrust perpendicular to the velocity vector is small compared to lift L and weight W.
5. The flight Mach number is less than the drag divergence Mach number, and should be in the range between 0.7 and 0.85.
6. The acceleration of the aircraft is small due to the steady-flight condition, so $\dot{v} \approx 0$.
7. The specific fuel consumption S_{FC} is a function of outside air temperature and flight Mach number and is given by (6).
8. Without loss of generality, the initial horizontal position is assumed to be $x(0) = 0$ and the final position $x(t_f) = x_d$.

Noting that $M_\infty = \frac{v}{c}$, where c is the speed of sound, and letting

$$A = A^* \sqrt{T^\circ_{FL}/T^\circ_{SL}}$$

equation (6) reduces to

$$S_{FC} = A\left(1 + B\frac{v}{c}\right). \tag{35}$$

In light of assumptions 1–7, the simplified dynamic model of a cruising turbofan aircraft

$$\begin{aligned} \dot{x} &= v \\ \dot{W} &= -S_{FC} T g \\ L &= W \\ T &= D \\ S_{FC} &= A\left(1 + B\frac{v}{c}\right) \\ D &= \frac{1}{2} C_{D,0} \rho S v^2 + \frac{2KW^2}{\rho S v^2}. \end{aligned} \tag{36}$$

In the dynamic model, x and W are the states and v acts as a control input. We can now proceed to formulate an OCP for the ECON mode for cruise flight of a turbofan aircraft.

3.3 Economy Mode Optimal Control Problem

In this section an Optimal Control Problem (OCP) for cruise flight of a turbofan aircraft is formulated. The economy (ECON) mode essentially means cruising at the most economical speed. This mode is based on the so-called cost index, which provides an effective and flexible tool to bias the FMS between the minimum energy consumption mode and the minimum flight time mode. The Direct Operating Cost (DOC) that is needed to be minimized is given by the functional

$$DOC = \int_0^{t_f} (C_t + C_f f)\, dt \tag{37}$$

where $C_t > 0$ and $C_f > 0$ are time-related costs and the cost of fuel, respectively. Recalling that

$$f = S_{FC} T$$

by (5) and since $C_f > 0$, minimizing DOC is equivalent to minimizing the cost function

$$J = \int_0^{t_f} (C_I + S_{FC} T)\, dt \tag{38}$$

Combining the cost functional (38) and flight dynamics (36) leads to the following OCP

$$
\begin{aligned}
J^* = &\inf_{v,t_f} \int_0^{t_f} (S_{FC}D + C_I)dt \\
&s.t. \\
&\dot{x} = v \\
&\dot{W} = -S_{FC}Dg \\
&D = \frac{1}{2}C_{D,0}\rho S v^2 + \frac{2KW^2}{\rho S v^2} \\
&S_{FC} = a(1 + b\frac{v}{c}) \\
&x(0) = 0,\ x(t_f) = x_d,\ W(0) = W_c
\end{aligned}
\tag{39}
$$

where the final time t_f is unspecified and the initial weight W_c is known.

Theorem 3. *The optimal solution to the OCP stated in (39) is the unique positive root of the quintic equation*

$$
(1 - J_W g)\left(\frac{BC_{D,0}\rho S}{c}v^5 + \frac{C_{D,0}\rho S}{2}v^4 - \frac{4BKW^2}{c\rho S}v - \frac{6KW^2}{\rho S}\right) - \frac{C_I}{A}v^2 = 0. \tag{40}
$$

Proof. The state equation for $x(t)$ in (39) is linear and therefore a unique solution exists for the state $x(t)$ for a given $v(t)$. The Hamiltonian of the OCP is given by

$$
H = (1 - J_W g)S_{FC}D + J_x v + C_I \tag{41}
$$

where J_W and J_x are the partial derivatives of the cost J with respect to the variables W and x, respectively.

Since H does not explicitly depend on time, according to the Pontryagin's minimum principle (see Chapter 2), necessary optimality conditions for free terminal time [24] lead to the following

Hamilton's equations

$$\frac{dJ_x}{dt} = -\frac{\partial H}{\partial x} \tag{42a}$$

$$\frac{dJ_W}{dt} = -\frac{\partial H}{\partial W} \tag{42b}$$

and the function $H(x, v, J_x, J_W)$ should reach its minimum at the optimal speed $v = v^*$, such that

$$H(x, v^*, J_x, J_W) = 0. \tag{43}$$

Combining equations (41) and (43) yields

$$(1 - J_W g)S_{FC}D + J_x v^* + C_I = 0. \tag{44}$$

From (42a), one can observe that $\dot{J}_x = 0$ which implies that J_x is a constant. From (42b) and (35), $\dot{J}_W$ is given by the following equation:

$$\dot{J}_W = (J_W g - 1)\frac{4A(Bv + c)KW}{\rho S c v^2}. \tag{45}$$

Furthermore, since the final weight W_f is unspecified, $J_W(t_f) = 0$.

The necessary condition for a minimum (inside the feasible domain $v > 0$) is

$$\frac{\partial H}{\partial v} = (1 - J_W g)\left(\frac{\partial S_{FC}}{\partial v}D + S_{FC}D_v\right) + J_x = 0 \tag{46}$$

where D_v denotes the partial derivative of drag D with respect to velocity v. The second-order sufficient condition for a minimum is verified for $v > 0$ if

$$\frac{\partial^2 H}{\partial v^2} = (1 - J_W g)\left(2\frac{\partial S_{FC}}{\partial v}D_v + S_{FC}D_{vv}\right) > 0. \tag{47}$$

From (47), using (2) and (35) we have

$$\frac{\partial^2 H}{\partial v^2} = (1 - J_W g)\left[\frac{AB}{c}\left(3C_{D,0}\rho S v + \frac{4KW^2}{\rho S v^3}\right) + A\left(C_{D,0}\rho S + \frac{12KW^2}{\rho S v^4}\right)\right] > 0. \tag{48}$$

It will be shown later that there exists a unique real positive solution of (46). Solving (46) for J_x yields

$$J_x = -(1 - J_W g)\left(\frac{\partial S_{FC}}{\partial v} D + S_{FC} D_v\right). \tag{49}$$

Replacing (49) in (44) yields

$$(1 - J_W g)\left(S_{FC} D - \frac{\partial S_{FC}}{\partial v} D v^* - S_{FC} D_v v^*\right) + C_I = 0. \tag{50}$$

Using the expressions (2) and (35) for drag and specific fuel consumption, respectively, transforms (50) into (40). It can be verified using Descartes' rule of signs that (40) has exactly one positive real root. □

3.4 Suboptimal Solution of Economy Mode Optimal Control Problem

In the literature [8, 13], J_W is often assumed to be 0 since the *instantaneous* cost does not change much with the aircraft weight. It will be shown later using the shooting method that this is a valid assumption for a turbofan aicraft. Setting $J_W = 0$, a suboptimal solution to the OCP can be obtained as the unique positive root of the quintic equation

$$\frac{B}{c} C_{D,0} \rho S v^5 + \frac{1}{2} C_{D,0} \rho S v^4 - \frac{C_I}{A} v^2 - \frac{4BKW^2}{c\rho S} v - \frac{6KW^2}{\rho S} = 0 \tag{51}$$

The main advantage of the suboptimal solution is that it allows one to use Newton's method to compute the cruising speed whereas the optimal solution requires computationally demanding methods such as the shooting method. This is due to the fact that the quadratic term in (40) depends on J_W, which is not constant.

3.5 Shooting Method

To validate the assumption $J_W \approx 0$, the shooting method is employed to solve (39). The augmented system is described by the following ODEs

$$\begin{aligned} \dot{x} &= v \\ \dot{W} &= -S_{FC} D g \\ \dot{J}_W &= (J_W g - 1)\frac{4 S_{FC} K W}{\rho S v^2} \end{aligned}$$

with the boundary conditions

$$\begin{aligned} x_0 &= 0 \\ x_{t_f} &= x_d \\ J_W(t_f) &= 0. \end{aligned}$$

This two-point boundary value problem (2PBVP) is solved in MATLAB using the `bvp4c` function. In the following section, we will compare the optimal and suboptimal solutions.

3.6 Simulations

3.6.1 Aircraft Model and Initial and Final Conditions

The aircraft model of the Boeing 737-800 will be used for simulations. The technical data and aircraft operating limits are presented in Table 3.1. Figs. 3.1–3.2 present the data obtained using the Boeing 737-800 flight simulator, which affirms that S_{FC} is an affine function in v. The initial velocity is 206.5 m/s ($M = 0.67$), and the value slowly decreases as the aicraft consumes fuel.

The initial and final conditions chosen for the simulations are presented in Table 3.2.

Table 3.1: Boeing 737-800 technical data

Length	39.47 m
Wingspan	34.32 m
Height	12.55 m
Wing area	124.6 m^2
Aspect ratio	9.44 m
Maximum takeoff mass	79016 kg
Ceiling	41000 ft
Cruise speed	Mach 0.789
Maximum speed	Mach 0.823
Range	5436 km
Zero-lift drag coefficient	0.020
Induced drag constant	0.055

Table 3.2: Simulation initial and final conditions

	Maximum range	ECON mode
Cruising altitude h, ft	30000	30000
Final position x_d, km	2075	2075
Initial mass W_c/g, kg	66286	66286
Cost index C_I, kg/s	0	0.3; 0.5

3.6.2 Simulation Results

The shooting method from Section 3.5 is used to obtain optimal state trajectories. Fig. 3.3 shows $J_W g$ as a function of the horizontal position x. One can observe that $J_W g$ is in fact small compared to 1 and decreases further as the cost index increases. Therefore, it is reasonable to assume $J_W g \approx 0$.

The results of the suboptimal and optimal solutions are compared with data accumulated from an FMS implemented in the Boeing 737 flight simulator for the cost index of $C_I = 0$. In Fig. 3.4 the true airspeed is plotted against the aircraft weight. The discrepancy between the simulator data and the obtained solutions is approximately 4 m/s. In the flight simulator, the minimization of the DOC is performed in intervals, which explains the step-like pattern. From Fig. 3.5 one can observe that the proposed algorithm allows for a more fuel-efficient maximum range flight than the one implemented in the flight simulator, resulting in 83.6 kg fuel savings by the end of 3.5 hours cruise. As expected, for $C_I = 0$ the suboptimal and optimal solutions yield the same result since

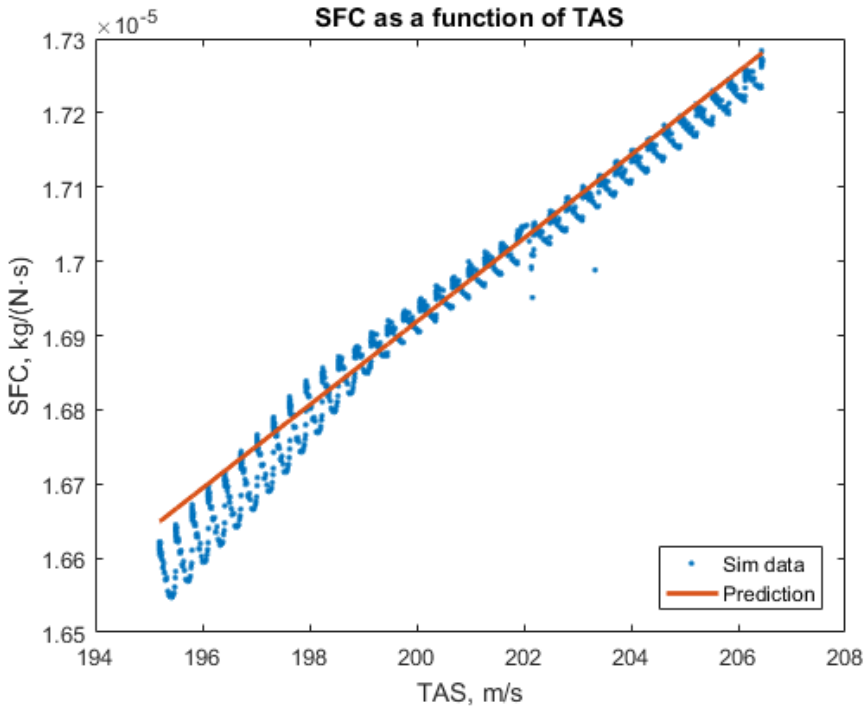

Figure 3.1: Specific fuel consumption as a function of true airspeed.

the quadratic term in (40) vanishes, and (40) reduces to (51). Larger cost index corresponds to the higher cruise speed as it is shown in Fig. 3.6. Moreover, Fig. 3.7 demonstrates that the discrepancy between the optimal and suboptimal solutions for any given weight becomes more significant as C_I increases.

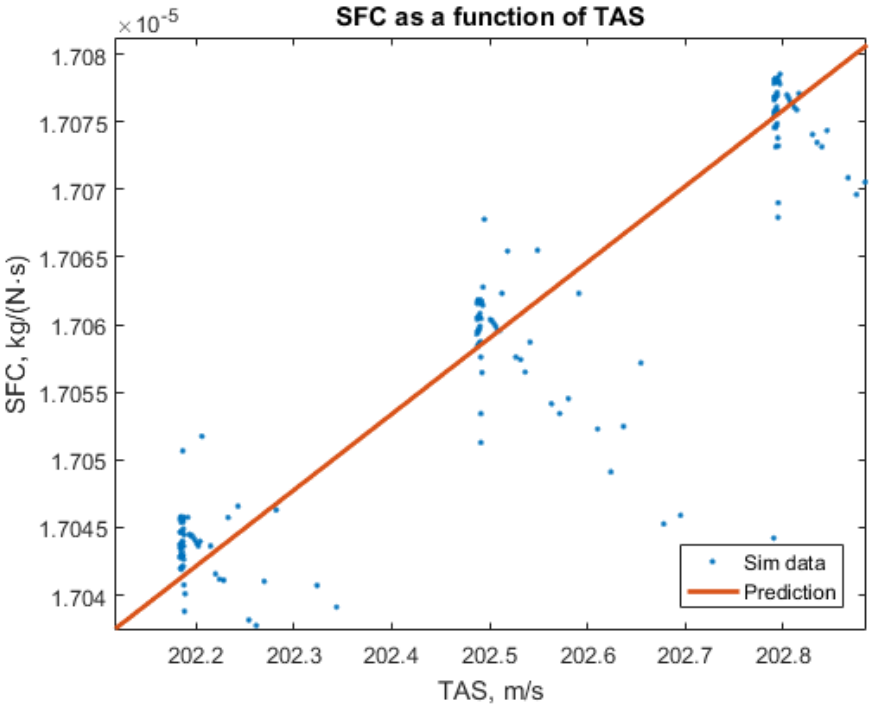

Figure 3.2: A close-up view of a section of the Fig. 3.1.

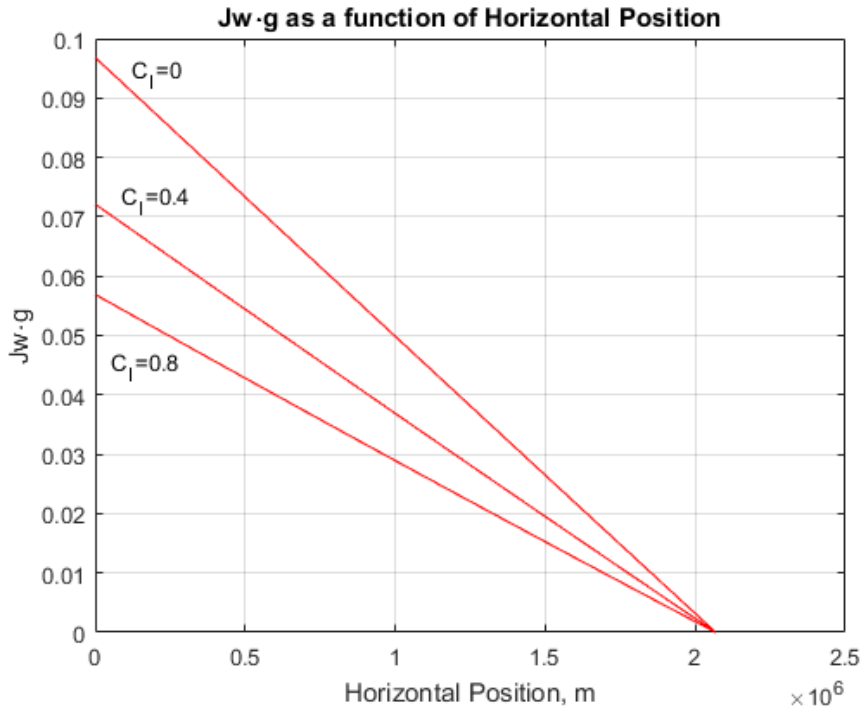

Figure 3.3: $J_W g$ as a function of the horizontal position.

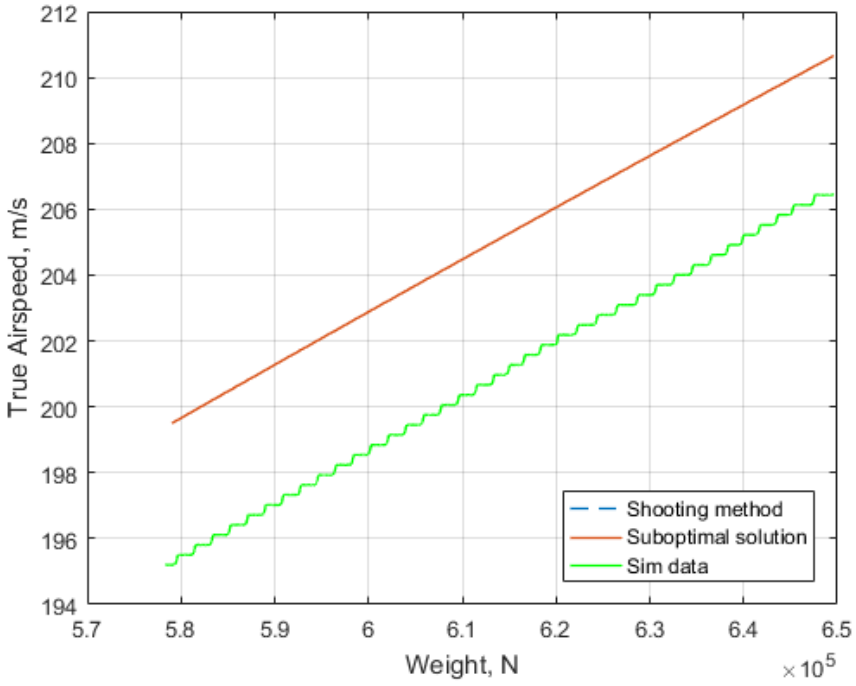

Figure 3.4: True airspeed as a function of the aircraft weight for $C_I = 0$.

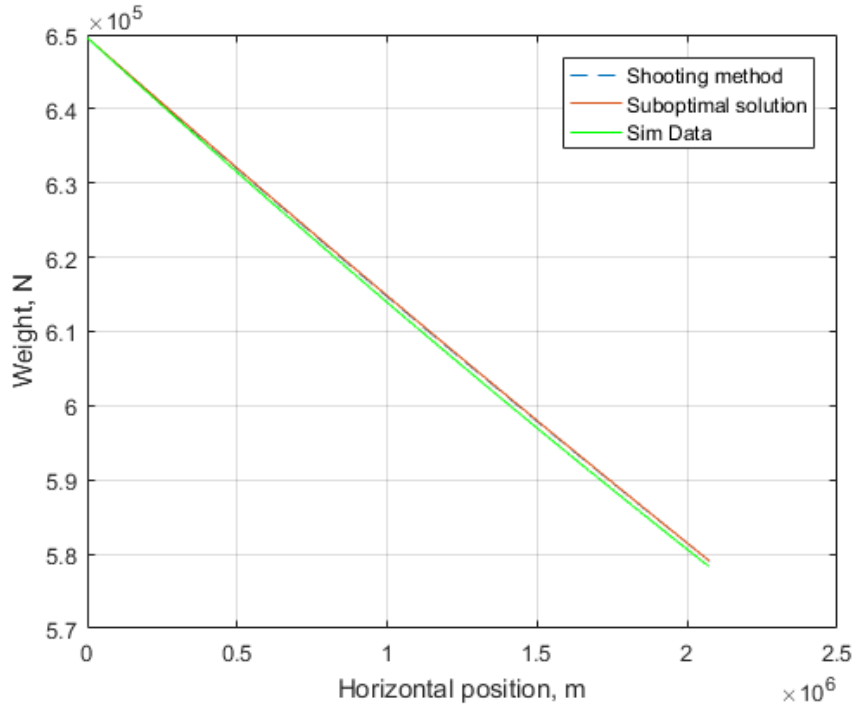

Figure 3.5: Weight as a function of the horizontal position for $C_I = 0$.

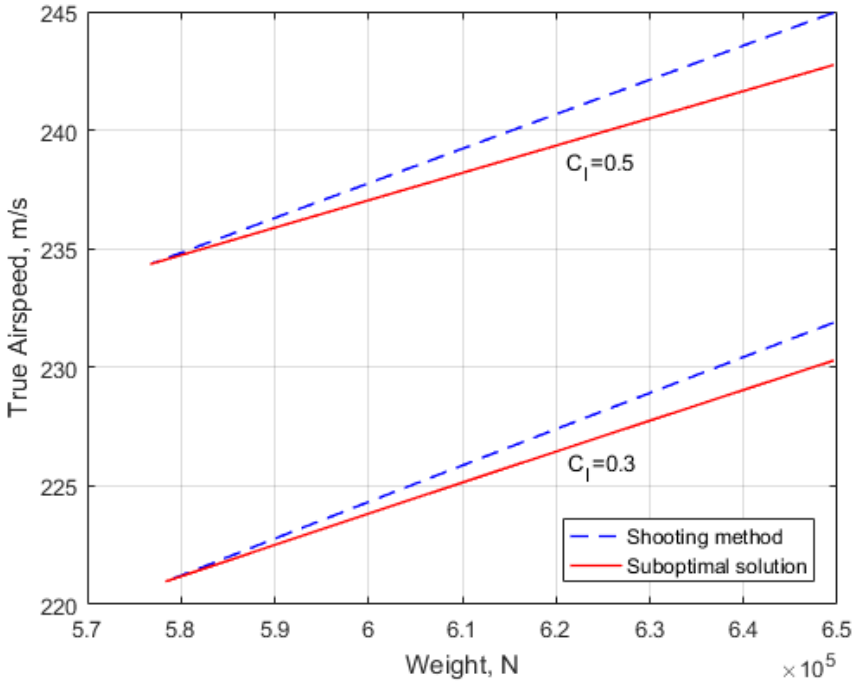

Figure 3.6: True airspeed as a function of the aircraft weight for different C_l.

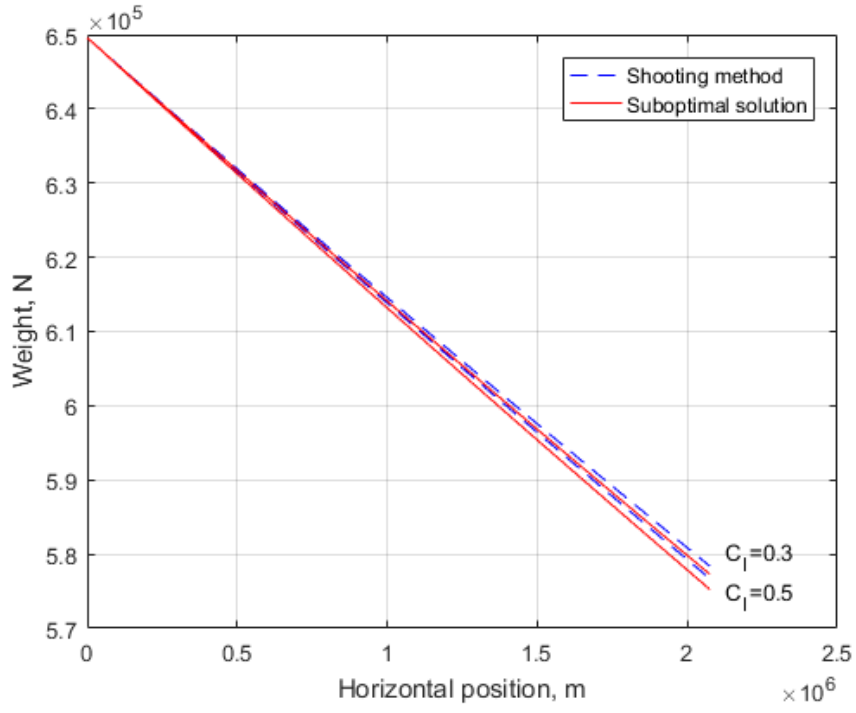

Figure 3.7: Weight as a function of the horizontal position for different C_l.

Chapter 4

Economy Mode and Maximum Endurance Optimal Solutions for All-Electric Aircraft

4.1 Introduction

The first manned flight of an airplane with an electric motor was the that of the HB-3 Brditschka in 1973. Initially, the aircraft was designed to use hydrocarbon fuel, but was later rebuilt to use electricity instead. However, the project did not go any further - the airplane could not stay airborne for more than 14 minutes.

The situation changed dramatically for the better in the mid-2000s. Several factors contributed to this. First, a more strict policy towards environmental pollution was adopted concerning not only air pollution, but also noise. Second, light and strong materials such as carbon fiber, suitable to be used in electric airplanes, became widespread. However, even the most advanced electric batteries are far behind the fossil fuel in terms of the specific energy density, i.e. the amount of energy stored per unit mass. It is therefore crucial to reduce the weight of such an aircraft as much as possible.

Apart from all-electric aircraft, another viable option is to use hydrogen to power a fuel cell to generate electricity to rotate the propeller shaft. Such aircraft include, for example, the Boeing-FCD

Project. Many companies are developing hybrid systems. One of the ideas is to design an aircraft that will take off and climb on electricity, then use the generator to drive electric fans and recharge onboard batteries while in cruise flight and finally descend and land as a pure electric aircraft.

In the following sections Optimal Control Problems (OCP) of ECON mode and maximum endurance wil be formulated and solved for all-electric aircraft.

4.2 Assumptions

Subsection 2.1.2 presented the longitudinal dynamic model of a cruising fuel-powered aircraft. For all-electric aircraft, the state equation for $\dot{W}$ appearing in (3) becomes irrelevant and is replaced by an appropriate equation for $\dot{Q}$ given by (10) or (14).

The following assumptions will be used to simplify the model:

1. The aircraft cruises at constant altitude, therefore, $\gamma = \dot{\gamma} = \dot{h} = 0$.
2. The angle of attack α is small, therefore, $\cos(\alpha) \approx 1$, $\sin(\alpha) \approx \alpha$.
3. The altitude, thrust, and speed of the aircraft are within the flight envelope.
4. The component of the thrust perpendicular to the velocity vector is small compared to lift L and weight W.
5. The acceleration of the aircraft is negligibly small due to a steady flight, so $\dot{v} \approx 0$.
6. The aircraft is flying below the drag divergence Mach number (which is a valid assumption for all-electric airplanes).
7. The air density is constant at fixed altitude.
8. Without loss of generality, the initial horizontal position is assumed to be $x(0) = 0$ and the final position $x(t_f) = x_d$.

In light of these assumptions, the simplified dynamic model of an all-electric aircraft is given

by

$$\begin{aligned} \dot{x} &= v \\ \dot{Q} &= -i = f(T, v, U) \\ L &= W \\ T &= D \\ D &= \frac{1}{2} C_{D,0} \rho S v^2 + \frac{2KW^2}{\rho S v^2}. \end{aligned} \tag{54}$$

In the dynamic model, x and Q are the states and v acts as a control input. Note, however, that since neither $\dot{x}$ nor $\dot{Q}$ depend explicitly on the states x and Q, only one state equation will be required to formulate a corresponding optimal control problem. For example, for maximum range we are only interested in the equation for $\dot{x}$ since x is the range variable.

4.3 Economy Mode Optimal Control Problem

For all-electric aircraft, the Direct Operating Cost (DOC) that we seek to minimize is given by the functional

$$DOC = \int_0^{t_f} (C_t + C_q i)\, dt \tag{55}$$

where $C_t > 0$ and $C_q > 0$ are time-related costs and the cost of the battery charge, respectively. Since $C_q > 0$, minimizing DOC is equivalent to minimizing the cost function

$$J = \int_0^{t_f} (C_I + i)\, dt \tag{56}$$

where $C_I = C_t/C_q$ is the cost index and acts as a trade-off parameter. A larger C_I corresponds to a higher true airspeed but results in the accelerated consumption of the battery charge. Conversely, a zero cost index implies cruising at a speed which minimizes the total energy consumption.

Combining the cost functional (56), the flight dynamics (54) and the expression for drag (2)

leads to the OCP

$$
\begin{aligned}
J^* = &\min_{v,t_f} \int_0^{t_f} (C_I + i)\, dt \\
&s.t. \\
&\dot{x} = v \\
&i = f(D, v, U) \\
&D = \frac{1}{2} C_{D,0} \rho S v^2 + \frac{2KW^2}{\rho S v^2} \\
&x(0) = 0,\ x(t_f) = x_d \\
&v(t) > 0,\ C_I \leq C_I^{crit}
\end{aligned}
\tag{57}
$$

where the final time t_f is unspecified. The exact form of the function $f(D, v, U)$ depends on a chosen battery model. The critical value of the coefficient index C_I^{crit} will be determined in the following theorem.

Theorem 4. *Assume the battery is ideal. For $C_I = 0$, the optimal solution to the OCP stated in (57) is given by*

$$
v_R = \sqrt{\frac{2W}{\rho S} \sqrt{\frac{K}{C_{D,0}}}} \tag{58}
$$

and the corresponding maximum range is

$$
R = \frac{Q_0 \eta U_{nom}}{2W \sqrt{C_{D,0} K}} \tag{59}
$$

where Q_0 is the initial battery charge. For $C_I > 0$, the optimal solution to the OCP stated in (57) exists for any $C_I \leq C_I^{crit}$ defined as

$$
C_I^{crit} = \frac{C_{D,0} \rho S v_{crit}^3}{\eta U_{nom}} - \frac{4KW^2}{\eta U_{nom} \rho S v_{crit}} \tag{60}
$$

where

$$
v_{crit} = \sqrt{\frac{\frac{Q_0 \eta U_{nom}}{x_d} + \sqrt{\left(\frac{Q_0 \eta U_{nom}}{x_d}\right)^2 - 4 C_{D,0} K W^2}}{C_{D,0} \rho S}} \tag{61}
$$

and is given by

$$v^* = X + \frac{1}{2}\sqrt{\frac{C_I \eta U_{nom}}{C_{D,0}\rho S X} - 4X^2} \tag{62}$$

where

$$X = \frac{1}{2}\sqrt{\frac{Z - \Delta_1/Z}{3C_{D,0}\rho S}}$$

$$Z = \left(\frac{\Delta_2 + \sqrt{\Delta_2^2 + 4\Delta_1^3}}{2}\right)^{1/3}$$

$$\Delta_1 = 48 C_{D,0} K W^2$$

$$\Delta_2 = 27 C_{D,0}\rho S (C_I \eta U_{nom})^2.$$

Proof. The state equation in (57) is linear and therefore a unique solution is guaranteed for the state $x(t)$ for a given $v(t)$. The dynamic system described by the state equation in (57) is clearly controllable.

For an ideal battery, the function $i = f(D, v, U)$ is obtained by combining the equation (10) for i and the flight dynamics (54) yielding

$$i = -\dot{Q} = \frac{Dv}{\eta U_{nom}}. \tag{63}$$

We can now proceed to form the Hamiltonian of the OCP which is given by

$$H = \frac{Dv}{\eta U_{nom}} + C_I + J_x v \tag{64}$$

where J_x is the partial derivative of the cost J with respect to the variable x. According to Pontryagin's minimum principle for time-invariant control systems (see Chapter 2), necessary optimality conditions for free terminal time [24] lead to the following Hamilton's equation

$$\frac{dJ_x}{dt} = -\frac{\partial H}{\partial x} \tag{65}$$

and the function $H(x, v, J_x)$ should reach its minimum at the optimal speed $v = v^*$, such that

$$H(x, v^*, J_x) = 0. \tag{66}$$

Combining equations (64) and (66) yields for the optimal input $v^\star$ the condition

$$\frac{Dv^*}{\eta U_{nom}} + C_I + J_x v^* = 0. \tag{67}$$

From (65), one can observe that $\dot{J}_x = 0$ which implies that J_x is a constant. The necessary condition for a minimum (inside the feasible domain $v > 0$) is

$$\frac{\partial H}{\partial v} = \frac{D_v v^* + D}{\eta U_{nom}} + J_x = 0 \tag{68}$$

where D_v denotes the partial derivative of drag D with respect to velocity v. Using (2) we have

$$\frac{\partial^2 H}{\partial v^2} = \frac{3C_{D,0}\rho S v + \frac{4KW^2}{\rho S v^3}}{\eta U_{nom}} > 0$$

for $v > 0$ and therefore we can conclude that H has a minimum at the solutions $v^\star$ of (68) if such solutions verify $v^\star > 0$. It will be shown later that there exists a unique real positive solution of (68). Solving (68) for J_x and using the expression (2) for drag leads to

$$J_x = \frac{1}{\eta U_{nom}} \left(\frac{2KW^2}{\rho S v^{*2}} - \frac{3}{2} C_{D,0} \rho S v^{*2} \right). \tag{69}$$

Replacing (69) in (67) yields

$$\frac{1}{\eta U_{nom}} \left(-C_{D,0}\rho S v^{*3} + \frac{4KW^2}{\rho S v^*} \right) + C_I = 0. \tag{70}$$

Multiplying both sides by $-\eta U_{nom} v^* < 0$ and rearranging terms yields the quartic equation

$$C_{D,0}\rho S v^{*4} - C_I \eta U_{nom} v^* - \frac{4KW^2}{\rho S} = 0. \tag{71}$$

The discriminant of this equation is

$$\Delta = -4^7 \left(C_{D,0}K\right)^3 \left(\rho S W\right)^6 - 27 C_{D,0}^2 \left(C_I \eta U_{nom}\right)^4 \left(\rho S\right)^8 < 0$$

which implies that (71) has two distinct real roots and two complex conjugate non-real roots. Further, according to Descartes' rule of signs, there is a unique positive real root $v^\star$ of (71) (see Chapter 2).

Zero cost index $C_I = 0$ corresponds to the maximum range solution and (71) reduces to

$$C_{D,0}\rho S v^{*4} - \frac{4KW^2}{\rho S} = 0 \tag{72}$$

whose solution is a constant velocity

$$v_R = \sqrt{\frac{2W}{\rho S}\sqrt{\frac{K}{C_{D,0}}}}.$$

This is the first result of the theorem statement. Equation (58) is the well-known expression for the maximum range speed (see [21] for example). Taking into account that the time rate of change of the battery charge given in (63) is constant for constant speed, the following equation must hold true for the maximum range

$$0 - Q_0 = \int_0^{t_R} \dot{Q} dt = \dot{Q} t_R. \tag{73}$$

From (73), using the expression for $\dot{Q}$ appearing in (63), the flight time for maximum range t_R is given by

$$t_R = \frac{Q_0 \eta U_{nom}}{D v_R}. \tag{74}$$

Since v_R is constant by (58), the maximum range can be determined as

$$R = v_R t_R = \frac{Q_0 \eta U_{nom}}{D}. \tag{75}$$

Using the expression (2) for drag evaluated at $v = v_R$ yields the maximum range equation (59).

For $C_I > 0$, equation (71) can be solved analytically [26] yielding the roots (see Chapter 2)

$$v_{1,2} = X \pm \frac{1}{2}\sqrt{\frac{C_I \eta U_{nom}}{C_{D,0}\rho S X} - 4X^2},$$

$$v_{3,4} = X \pm \frac{1}{2}\sqrt{-\frac{C_I \eta U_{nom}}{C_{D,0}\rho S X} - 4X^2}$$

where

$$X = \frac{1}{2}\sqrt{\frac{Z - \Delta_1/Z}{3C_{D,0}\rho S}}$$

$$Z = \left(\frac{\Delta_2 + \sqrt{\Delta_2^2 + 4\Delta_1^3}}{2}\right)^{1/3}$$

$$\Delta_1 = 48 C_{D,0} K W^2$$

$$\Delta_2 = 27 C_{D,0}\rho S (C_I \eta U_{nom})^2$$

and $Z > 0,\ (Z - \Delta_1/Z) > 0$ for $C_I > 0$. As mentioned before, according to Descartes' rule of signs, there is a unique positive real root of (71). It can also be shown using the same rule that there is a unique negative real root. Therefore, among the solutions $v_{1,2}$ and $v_{3,4}$ there are exactly one positive real root, one negative real root and two complex conjugate roots. It will be proved now by contradiction that the roots $v_{1,2}$ are real. Assume $v_{1,2}$ are complex conjugate. This implies

$$\frac{C_I \eta U_{nom}}{C_{D,0}\rho S X} - 4X^2 < 0.$$

If $v_{1,2}$ are complex conjugate then $v_{3,4}$ must be real, and the following must hold true

$$-\frac{C_I \eta U_{nom}}{C_{D,0}\rho S X} - 4X^2 > 0$$

and, consequently,

$$-\frac{C_I \eta U_{nom}}{C_{D,0}\rho S X} > 4X^2 > \frac{C_I \eta U_{nom}}{C_{D,0}\rho S X}$$

which does not hold for $X > 0$. Therefore, the assumption must be wrong, and $v_{1,2}$ must be real

roots. Let

$$v^* = X + \frac{1}{2}\sqrt{\frac{C_I \eta U_{nom}}{C_{D,0}\rho S X} - 4X^2}.$$

Since this is the largest of the real roots then it must be the positive real root.

We now derive an expression for the critical cost index C_I^{crit}. This determines the corresponding critical velocity v_{crit} at which the aircraft may cruise to reach the desired final top of descent position. Flying at speed exceeding v_{crit} will result in the complete battery depletion before arriving at that point. Replacing R by x_d and D by $D_{crit} = \frac{1}{2}C_{D,0}\rho S v_{crit}^2 + \frac{2KW^2}{\rho S v_{crit}^2}$ in (75) yields a biquadratic equation

$$\frac{1}{2}C_{D,0}\rho S v_{crit}^4 - \frac{Q_0 \eta U_{nom}}{x_d} v_{crit}^2 + \frac{2KW^2}{\rho S} = 0 \tag{76}$$

which has the positive real solution

$$v_{crit} = \sqrt{\frac{\frac{Q_0 \eta U_{nom}}{x_d} + \sqrt{\left(\frac{Q_0 \eta U_{nom}}{x_d}\right)^2 - 4C_{D,0}KW^2}}{C_{D,0}\rho S}}.$$

Note that v_{crit} is well defined (i.e, it is a positive real number) since $x_d \leq R$, where R is given by equation (59). Solving (71) for C_I using $v = v_{crit}$ yields the following expression for the critical cost index

$$C_I^{crit} = \frac{C_{D,0}\rho S v_{crit}^3}{\eta U_{nom}} - \frac{4KW^2}{\eta U_{nom}\rho S v_{crit}}.$$

□

Equation (62) is an analytical expression for the True Airspeed (TAS) that minimizes DOC for the cruise flight segment. It should be noted that the obtained speed, as well as the correspoding electric current, remain the same for the entire cruise segment at constant altitude because the battery voltage U was assumed to be constant and equal to U_{nom}. In practice, the optimal speed would decrease slowly as the output voltage drops.

In [23], the authors studied the effects of the current amplitude on the battery capacity described by Peukert's law. They concluded that this law cannot be employed to accurately estimate the

SOC of a battery unless it is discharged at a constant current and constant temperature, which is rarely the case in most practical applications. When the Peukert constant is $n = 1$ (i.e., the capacity is independent of the current), the expression for the maximum range R developed by the author of [18] reduces to (59). It was established in [23] that making $n > 1$ usually leads to an underestimation of the remaining battery capacity.

Having an analytical expression for the maximum range allows one to obtain sensitivities of the maximum range R with respect to the battery voltage U and aircraft weight W as

$$\frac{\partial R}{\partial U} = \frac{Q_0 \eta}{2W\sqrt{C_{D,0}K}} \tag{77a}$$

$$\frac{\partial R}{\partial W} = -\frac{Q_0 \eta U_{nom}}{2W^2\sqrt{C_{D,0}K}}. \tag{77b}$$

Theorem 5. *Assume the battery has internal resistance $r > 0$. For $i \in [0; \frac{U_{nom}}{2r})$ and $C_I \geq 0$, the optimal solution v^* to the OCP stated in (57) for cruise flight at constant altitude is a unique positive root (if it exists) of the nonlinear equation*

$$\begin{aligned} &\left(C_I + \frac{U_{nom}}{2r}\right)\sqrt{(\eta U_{nom})^2 - 2\eta r\left(C_{D,0}\rho S v^{*3} + \frac{4KW^2}{\rho S v^*}\right)} \\ &= \frac{\eta U_{nom}^2}{2r} + \frac{1}{2}C_{D,0}\rho S v^{*3} - \frac{6KW^2}{\rho S v^*}. \end{aligned} \tag{78}$$

For $C_I = 0$, the maximum range is

$$R = \frac{2\eta r Q_0 v_R}{\eta U_{nom} - \sqrt{(\eta U_{nom})^2 - 2\eta r\left(C_{D,0}\rho S v_R^3 + \frac{4KW^2}{\rho S v_R}\right)}} \tag{79}$$

where the speed for maximum range v_R is a unique positive root (if it exists) of

$$\frac{U_{nom}}{2r}\sqrt{(\eta U_{nom})^2 - 2\eta r\left(C_{D,0}\rho S v^3 + \frac{4KW^2}{\rho S v}\right)} = \frac{\eta U_{nom}^2}{2r} + \frac{1}{2}C_{D,0}\rho S v^3 - \frac{6KW^2}{\rho S v}. \tag{80}$$

Proof. For a battery with internal resistance, the function $i = f(D, v, U)$ is obtained by combining

the equation (14) for i and the flight dynamics (54) yielding

$$i = -\dot{Q} = \frac{U_{nom}}{2r} - \frac{\sqrt{(\eta U_{nom})^2 - 4\eta r D v}}{2\eta r}. \tag{81}$$

The problem is well-posed for $i \in [0; \frac{U_{nom}}{2r})$ where the upper limit corresponds to the value of electric current for which the cost function J is independent of the control input v. In fact, if $i = \frac{U_{nom}}{2r}$, then $\frac{\sqrt{(\eta U_{nom})^2 - 4\eta r D v}}{2\eta r} \equiv 0$. The Hamiltonian of the OCP can be written as

$$H = \frac{U_{nom}}{2r} - \frac{\sqrt{(\eta U_{nom})^2 - 4\eta r D v}}{2\eta r} + J_x v + C_I. \tag{82}$$

Since the Hamiltonian is explicitly independent of time and the terminal time is free, then, according to Pontryagin's minimum principle, necessary optimality conditions [24] lead to the following Hamilton's equation (see Chapter 2)

$$\frac{dJ_x}{dt} = -\frac{\partial H}{\partial x} = 0, \tag{83}$$

and the optimal control input v^* minimizes the Hamiltonian (82) over all feasible values of v such that

$$H(x, v^*, J_x) = 0. \tag{84}$$

Combining equations (82) and (84) yields

$$H = \frac{U_{nom}}{2r} - \frac{\sqrt{(\eta U_{nom})^2 - 4\eta r D v^*}}{2\eta r} + J_x v^* + C_I = 0. \tag{85}$$

From (83), it is evident that J_x is a constant. The necessary condition for a minimum inside the feasible set is

$$\frac{\partial H}{\partial v} = \frac{D_v v^* + D}{\sqrt{(\eta U_{nom})^2 - 4\eta r D v^*}} + J_x = 0. \tag{86}$$

One can verify that $\sqrt{(\eta U_{nom})^2 - 4\eta r D v} > 0$ for $i \neq \frac{U_{nom}}{2r}$ by replacing U_{nom} and Dv by $U + ir$

and ηUi, respectively, in (86). From (86) we have

$$\frac{\partial^2 H}{\partial v^2} = \frac{(D_{vv}v^* + 2D_v)X + \frac{2\eta r(D_v v^* + D)^2}{X}}{X^2} > 0 \tag{87}$$

where $X = \sqrt{(\eta U_{nom})^2 - 4\eta r D v^*}$. Equation (87) holds for $v > 0$ and therefore H attains its minimum at the solution v^*. Solving (86) for J_x and using the expression (2) for drag leads to

$$J_x = \frac{-3C_{D,0}\rho^2 S^2 v^{*4} + 4KW^2}{2\rho S v^{*2}\sqrt{(\eta U_{nom})^2 - 2\eta r\left(C_{D,0}\rho S v^{*3} + \frac{4KW^2}{\rho S v^*}\right)}}. \tag{88}$$

Replacing (88) in (85) yields

$$\begin{aligned} &C_I + \frac{U_{nom}}{2r} - \frac{\sqrt{(\eta U_{nom})^2 - 2\eta r\left(C_{D,0}\rho S v^{*3} + \frac{4KW^2}{\rho S v^*}\right)}}{2\eta r} \\ &+ \frac{-3C_{D,0}\rho^2 S^2 v^{*4} + 4KW^2}{2\rho S v^*\sqrt{(\eta U_{nom})^2 - 2\eta r\left(C_{D,0}\rho S v^{*3} + \frac{4KW^2}{\rho S v^*}\right)}} = 0. \end{aligned} \tag{89}$$

Multiplying both sides by

$$\sqrt{(\eta U_{nom})^2 - 2\eta r\left(C_{D,0}\rho S v^{*3} + \frac{4KW^2}{\rho S v^*}\right)} \neq 0$$

and rearranging terms yields

$$\begin{aligned} &\left(C_I + \frac{U_{nom}}{2r}\right)\sqrt{(\eta U_{nom})^2 - 2\eta r\left(C_{D,0}\rho S v^{*3} + \frac{4KW^2}{\rho S v^*}\right)} \\ &= \frac{\eta U_{nom}^2}{2r} + \frac{1}{2}C_{D,0}\rho S v^{*3} - \frac{6KW^2}{\rho S v^*}, \end{aligned}$$

which is the first result of the statement of the theorem. It will be shown later that if a solution to (78) exists, then it is unique.

By setting $C_I = 0$, (78) reduces to (79) and the maximum range speed v_R is obtained. Taking into account that the time rate of change of the battery charge given in (81) is constant for constant

speed and fixed altitude, the following equation must hold for the maximum range

$$0 - Q_0 = \int_0^{t_R} \dot{Q} dt = \dot{Q} t_R. \tag{90}$$

From (90), using the expression for $\dot{Q}$ appearing in (81), the flight time for maximum range t_R is given by

$$t_R = \frac{2\eta r Q_0}{\eta U_{nom} - \sqrt{(\eta U_{nom})^2 - 2\eta r \left(C_{D,0} \rho S v_R^3 + \frac{4KW^2}{\rho S v_R} \right)}}. \tag{91}$$

Since the optimal velocity is constant, the maximum range can be obtained as

$$R = v_R t_R = \frac{2\eta r Q_0 v_R}{\eta U_{nom} - \sqrt{(\eta U_{nom})^2 - 2\eta r \left(C_{D,0} \rho S v_R^3 + \frac{4KW^2}{\rho S v_R} \right)}}.$$

We now prove by contradiction that if there exists a solution to (78), then it is unique. Consider the function inside the square root on the left-hand side of (78)

$$LH_{sq} = (\eta U_{nom})^2 - 2\eta r \left(C_{D,0} \rho S v^3 + \frac{4KW^2}{\rho S v} \right). \tag{92}$$

Function $LH_{sq} > 0$ for $i \neq \frac{U_{nom}}{2r}$ as it was shown earlier. Its first derivative with respect to v is

$$\frac{\partial LH_{sq}}{\partial v} = -2\eta r \left(3 C_{D,0} \rho S v^2 - \frac{4KW^2}{\rho S v^2} \right)$$

and the second derivative with respect to v is

$$\frac{\partial^2 LH_{sq}}{\partial v^2} = -2\eta r \left(6 C_{D,0} \rho S v + \frac{8KW^2}{\rho S v^3} \right) < 0$$

which implies that the function LH_{sq} has one maximum at $v = \sqrt{\frac{2W}{\rho S}} \sqrt{\frac{K}{3C_{D,0}}}$ which can be found by setting $\frac{\partial LH_{sq}}{\partial v} = 0$. Consequently, the function $LH = \sqrt{LH_{sq}}$ also has one maximum at $v > 0$. Consider now the function on the right-hand side of (78)

$$RH = \frac{\eta U_{nom}^2}{2r} + \frac{1}{2} C_{D,0} \rho S v^3 - \frac{6KW^2}{\rho S v}. \tag{93}$$

It is monotonically increasing for $v > 0$ since

$$\frac{\partial RH}{\partial v} = \frac{3}{2} C_{D,0} \rho S v^2 + \frac{6KW^2}{\rho S v^2} > 0.$$

Therefore, there exists three possible combinations of solutions of (78):

A: Two solutions, at least one of which is at $v < \sqrt{\frac{2W}{\rho S}\sqrt{\frac{K}{3C_{D,0}}}}$.

B: One solution at $v > 0$.

C: No solution.

One can verify that J_x is negative for $v > \sqrt{\frac{2W}{\rho S}\sqrt{\frac{K}{3C_{D,0}}}}$ and positive for $v < \sqrt{\frac{2W}{\rho S}\sqrt{\frac{K}{3C_{D,0}}}}$ by (88). The positive constant J_x implies that C_I is negative by (85) which contradicts the problem statement. Therefore, we can conclude that there is either one solution (Case B) or no solution at all (Case C). □

The obtained speed, as well as the correspoding electric current, remain constant for the entire cruise segment at fixed altitude since all the coefficients in (78) are time independent. Equation (78) can be solved by means of numerical methods such as for example Newton's method.

4.4 Maximum Endurance Optimal Control Problem

Expressions for maximum endurance and the correspoding velocity of an all-electric airplane (assuming zero internal resistance) can be found, for example, in [18]. However, these expressions were not obtained within the optimal control framework. In this section, an OCP to maximize the endurance is formulated and solved. The OCP involves maximizing the amount of time that the aircraft can stay airborne. Since the constraint on the the final position is lifted, the state equation for the horizontal position $\dot{x}$ appearing in (54) becomes irrelevant. The following OCP can now be

formulated

$$
\begin{aligned}
J^* = &\max_{v,t_f} \int_0^{t_f} dt \\
&s.t. \\
&\dot{Q} = f(D, v, U) \\
&D = \frac{1}{2} C_{D,0} \rho S v^2 + \frac{2KW^2}{\rho S v^2} \\
&v(t) > 0,\ Q(0) = Q_0,\ Q(t_f) = 0
\end{aligned}
\tag{94}
$$

where the final time t_f is unspecified. The exact form of the function $f(D, v, U)$ depends on a chosen battery model.

Theorem 6. *Assume the battery is ideal. The optimal solution to the OCP stated in (94) is given by*

$$
v_E = \sqrt{\frac{2W}{\rho S} \sqrt{\frac{K}{3C_{D,0}}}} \tag{95}
$$

and the maximum endurance of an all-electric airplane is

$$
E = \frac{3^{3/4} \eta U_{nom} Q_0 \sqrt{\rho S}}{2^{5/2} C_{D,0}^{1/4} K^{3/4} W^{3/2}}. \tag{96}
$$

Proof. For an ideal battery, the state equation for $\dot{Q} = f(D, v, U)$ is given by (63) and corresponds to a function that is continuously differentiable with bounded derivative with respect to the control input $v > 0$. This implies that this function is locally Lipschitz for admissible inputs. Therefore, there exists a local unique solution to the differential equation in (94). The state Q is also locally controllable.

The Hamiltonian of the OCP (94) is

$$
H = 1 - J_Q \frac{Dv}{\eta U_{nom}} \tag{97}
$$

where J_Q is the partial derivative of the cost J with respect to the variable Q. According to Pontryagin's maximum principle for time-invariant control systems (see Chapter 2), for the control input v

to be optimal, the following must hold

$$H(Q, v^*, J_Q) = 0. \tag{98}$$

Combining equations (97) and (98) yields

$$1 - J_Q \frac{Dv^*}{\eta U_{nom}} = 0. \tag{99}$$

Solving (99) for J_Q leads to

$$J_Q = \frac{\eta U_{nom}}{Dv^*} \tag{100}$$

which implies that J_Q is positive. The necessary condition for optimality inside the feasible domain $v > 0$ is

$$\frac{\partial H}{\partial v} = -J_Q \left(\frac{D_v v^*}{\eta U_{nom}} + \frac{D}{\eta U_{nom}} \right) = 0. \tag{101}$$

The second-order sufficient condition for a maximum is verified for $v > 0$ since using (2) we have

$$\frac{\partial^2 H}{\partial v^2} = -\frac{J_Q}{\eta U_{nom}} \left(3C_{D,0}\rho S v^* + \frac{4KW^2}{\rho S v^{*3}} \right) < 0. \tag{102}$$

Using the expression (2) for drag and solving (101) for v^* yields the first result of the theorem

$$v_E = \sqrt{\frac{2W}{\rho S}\sqrt{\frac{K}{3C_{D,0}}}}.$$

Again, using the expression (2) for drag and evaluating the expression for $\dot{Q}$ appearing in (63) at $v = v_E$ yields the electric current corresponding to the maximum endurance speed

$$\dot{Q}_E = -\frac{2^{5/2} C_{D,0}^{1/4} K^{3/4} W^{3/2}}{3^{3/4} \eta U_{nom} \sqrt{\rho S}}. \tag{103}$$

From (103) and the assumption of constant altitude it is evident that $\dot{Q}_E$ is constant. The following

must hold for the maximum endurance

$$0 - Q_0 = \int_0^{t_f} \dot{Q}_E dt = \dot{Q}_E(t_f - 0) = \dot{Q}_E E \tag{104}$$

where E is the maximum endurance. Solving (104) for E and using (103) yields the second result of the theorem. □

Equation (95) is the same as the one that was obtained in [18]. The expression for the maximum endurance E developed by the author of [18] reduces to (95) when the discharge parameter n considered in his work is equal to 1.

Theorem 7. *Assume the battery has internal resistance. The optimal solution to the OCP stated in (94) is given by*

$$v_E = \sqrt{\frac{2W}{\rho S}\sqrt{\frac{K}{3C_{D,0}}}}$$

and the maximum endurance of an all-electric airplane is

$$E = \frac{2\eta r Q_0}{\eta U_{nom} - \sqrt{(\eta U_{nom})^2 - \frac{2^{9/2} C_{D,0}^{1/4} K^{3/4} W^{3/2} \eta r}{3^{3/4}\sqrt{\rho S}}}}. \tag{105}$$

Proof. For a battery with internal resistance, the state equation $\dot{Q} = f(D, v, U)$ is described by (81) and is continuously differentiable with bounded derivative on the control input $v > 0$, meaning that the function is locally Lipschitz for admissible inputs $v > 0$ and there exists a local unique solution to the differential equation in (94). The state Q is also locally controllable.

The Hamiltonian of the OCP (94) is

$$H = 1 - J_Q \left(\frac{U_{nom}}{2r} - \frac{\sqrt{(\eta U_{nom})^2 - 4\eta r D v}}{2\eta r} \right). \tag{106}$$

Following the same steps as in the proof of the previous theorem, the control input v is optimal if the following holds true

$$H(Q, v^*, J_Q) = 0. \tag{107}$$

From Hamilton's equations

$$\frac{dJ_Q}{dt} = -\frac{\partial H}{\partial Q} = 0 \tag{108}$$

one can see that J_Q is constant. Combining equations (106) and (107) yields

$$1 - J_Q \left(\frac{U_{nom}}{2r} - \frac{\sqrt{(\eta U_{nom})^2 - 4\eta r D v^*}}{2\eta r} \right) = 0. \tag{109}$$

Solving (109) for J_Q leads to

$$J_Q = \frac{2\eta r}{\eta U_{nom} - \sqrt{(\eta U_{nom})^2 - 4\eta r D v^*}} \tag{110}$$

which implies that J_Q is positive since it was proved in Section 4.3 that

$$\eta U_{nom} - \sqrt{(\eta U_{nom})^2 - 4\eta r D v} > 0$$

for $i \neq \frac{U_{nom}}{2r}$. Equation (110) is well-defined for admissible v since $Dv \neq 0$ for all $v > 0$. The necessary condition for optimality inside the feasible domain $v > 0$ is

$$\frac{\partial H}{\partial v} = -J_Q \left(\frac{D_v v^* + D}{\sqrt{(\eta U_{nom})^2 - 4\eta r D v^*}} \right) = 0. \tag{111}$$

The second-order sufficient condition for a maximum is verified for $v > 0$ because

$$\frac{\partial^2 H}{\partial v^2} = -J_Q \frac{(D_{vv} v^* + 2D_v) X + \frac{2\eta r (D_v v^* + D)^2}{X}}{X^2} < 0 \tag{112}$$

where $X = \sqrt{(\eta U_{nom})^2 - 4\eta r D v^*} \neq 0$ as it was shown in the proof of Theorem 5. Using the expression (2) for drag and solving (111) for v^* yields the speed for maximum endurance

$$v_E = \sqrt{\frac{2W}{\rho S} \sqrt{\frac{K}{3C_{D,0}}}}$$

which is independent of the battery internal resistance r.

The electric current corresponding to the maximum endurance speed can be found using the

expression (2) for drag and evaluating the expression for $\dot{Q}$ appearing in (81) at $v = v_E$

$$\dot{Q}_E = -\frac{U_{nom}}{2r} + \frac{\sqrt{(\eta U_{nom})^2 - \frac{2^{9/2} C_{D,0}^{1/4} K^{3/4} W^{3/2} \eta r}{3^{3/4}\sqrt{\rho S}}}}{2\eta r} \tag{113}$$

which is constant for fixed altitude. Using (113) and solving (104) for E we recover the maximum endurance equation (105). □

As one can see, the maximum endurance speed obtained for the two aforementioned battery models is exactly the same. This is an expected result. The maximum endurance speed corresponds to the minimim of the function P_R given by (7), which does not depend on battery parameters.

4.5 Simulations

4.5.1 Aircraft Model and Initial and Final Conditions

The model of the Airbus E-Fan 1.0 (see Fig. 4.1 [3]) is used for simulations. The E-Fan is an all-electric technology demonstrator two-seater aircraft of composite material structure. Its lithium-ion polymer batteries mounted on the inboard section of the wing supply power to two electric ducted fan motors at the rear. The aircraft is specifically designed for short-term flights such as pilot training, glider towing and aerobatics. The technical data is presented in Table 4.1.

The wing area $S = 10\ m^2$ is estimated based on the available images of the E-Fan 1.0 [3]. The zero-lift drag coefficient $C_{D,0} = 0.025$ was chosen so as to be within the range typical for small general aviation aircraft [31]. The induced drag constant K is obtained based on the known lift-to-drag ratio L/D using the following relationships [21]:

$$\begin{aligned} L/D &= \frac{1}{2}\sqrt{\pi e \text{Æ} R / C_{D,0}} \\ K &= 1/(\pi e \text{Æ} R) \end{aligned} \tag{114}$$

where e is the span efficiency factor and $\text{Æ}R$ is the aspect ratio. Solving (114) for the two unknowns K and $(\pi e \text{Æ} R)$ yields the following value for the induced drag constant: $K = 0.039$. The total system efficiency $\eta = 0.68$ was chosen in accordance with [19] and represents the efficiency of a

Figure 4.1: E-Fan technology demonstrator.

typical on-board conversion chain, starting from the primary energy source (the battery) and ending with the propeller.

In 2015, the E-Fan 1.0 crossed the English Channel, completing the 74 kilometer flight from Lydd, England to Calais, France, in about 37 minutes. The flight route is shown in Fig. 4.2. Overall, the E-Fan utilized its on-board battery system for 53 min spending 79 % of the total energy of the batteries by the end of the flight [3]. The initial and final conditions were chosen to simulate this flight and are presented in Table 4.2.

4.5.2 Simulation Results

The use of a battery model with internal resistance provides more precise results compared to those obtained using an ideal battery ($r = 0$). For an ideal battery, using the formulas (59) and (96) yields the maximum range 193 km and the maximum endurance 100 min. These values are significantly overestimated since (80) and (105) yield the maximum range 173 km and the maximum endurance 92 min. The relative errors are equal to 11% and 10%, respectively. The maximum endurance is only 17 min higher than that presented in the Table 4.1, which is an encouraging result given that some important aircraft performance characteristics are based on estimates.Moreover, one

Table 4.1: E-Fan 1.0 technical data

Wing span	9.5 m
Length	6.67 m
Height	2 m
Wing area	10* m^2
Maximum take-off weight	600 kg
Lift/Drag ratio	16
Maximum electric motor power	60 kW
Battery system	2982 cells
Energy density per battery cell	207 $Wh/cell$
Battery cell internal resistance	30* mΩ
Total available energy	29 kWh
Total battery weight	167 kg
Endurance	up to 75 min
Take-off speed	110 km/h
Cruise speed	160 km/h
Maximum speed	220 km/h
Static thrust	1.5 kN
Total system efficiency	0.68*
Parasitic drag coefficient	0.025*
Induced drag constant	0.039*

All values are from [3, 29, 30] except those marked by an (*), which are estimates.

Table 4.2: Simulation initial and final conditions

Cruising altitude h	3500 ft
Final position x_d	74 km
Initial charge Q_0	141 120 C (39.2 $A \cdot h$)
Weight W	600 kg

needs to bear in mind that the maximum endurance refers to the maximum theoretically achievable endurance (assuming complete battery depletion and cruising at a speed close to the stall speed) whereas the endurance defined by the manufacturer is practically attainable.

Since $x_d \leq R$ there exists an optimal velocity to reach the desired final position. The critical cost index C_I^{crit} appearing in the statement of the Theorem 4 is computed using (60) and is equal to 288 A.

The graph shown in Fig. 4.3 gives the optimal cruise velocity as a function of cost index. One can observe that larger values of C_I correspond to higher cruising velocity. Also, as C_I increases

Figure 4.2: E-Fan cross-Channel flight route.

the discrepancy between speeds obtained using different battery models also increases, thus making an improved battery model more relevant.

The Pareto-optimal trade-off curve between the final optimal time and the amount of charge consumed for different values of C_I and corresponding optimal TAS is shown in Fig. 4.4. It is clear from the plot that, as expected, if C_I increases the time of flight decreases and the charge depleted increases. Essentially, the cost index C_I allows to trade-off between minimizing travel time and minimizing the amount of the battery charge used. As expected, the curve corresponding to the battery with an internal resistance is above the ideal battery curve, implying the increased battery charge consumption for the same amount of time spent in cruise.

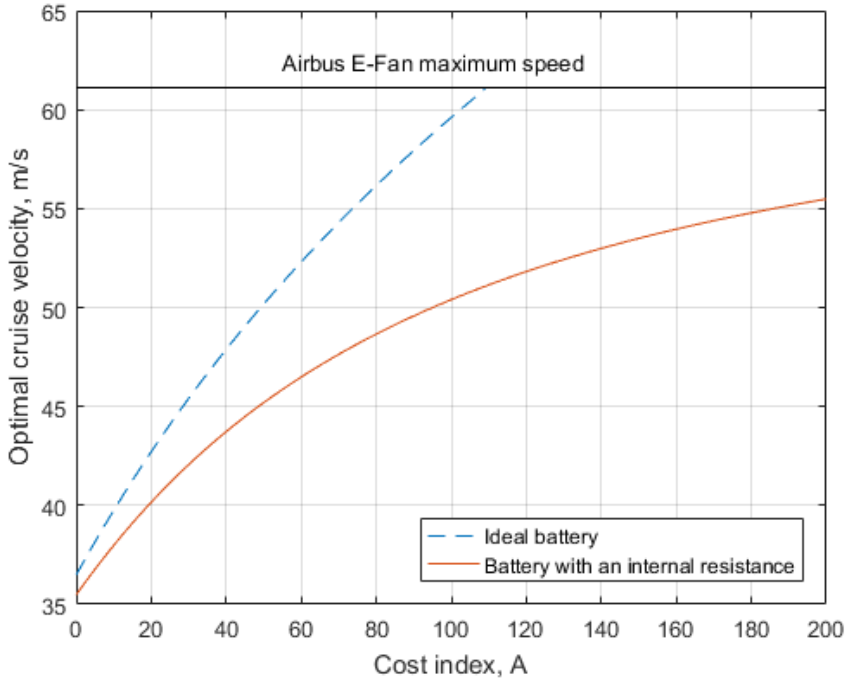

Figure 4.3: Comparison of velocities obtained for different battery models.

It can be concluded that the discrepancy between the two battery models does introduce significant changes in the optimal cruising speed, maximum range and maximum endurance. Therefore, the numerical solution is preferable to use unless the internal resistance is small and can be neglected as is the case with high-quality lithium polymer cells.

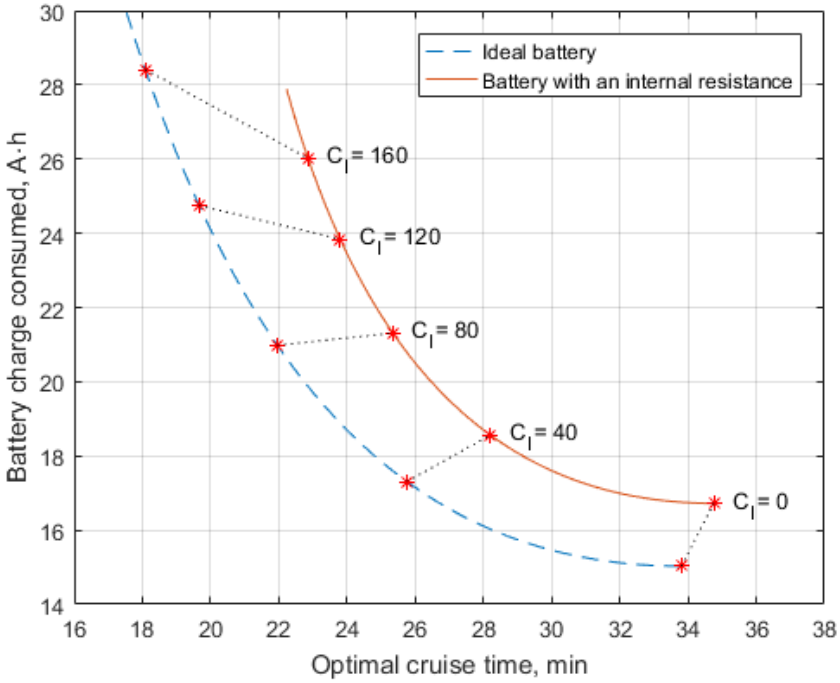

Figure 4.4: Pareto-optimal trade-off curve.

Chapter 5

Conclusions and Future Work

5.1 Conclusions

This thesis has presented a method to solve optimal control problems pertaining to the Economy Mode of turbofan and all-electric aircraft. Numerical and/or analytical optimal solutions (whenever possible) for the true air speed, maximum range and maximum endurance have been found using Pontryagin's minimum principle.

For the Boeing 737-800 turbofan aircraft, the obtained results demonstrated that the proposed method fits the flight simulator data well. For the Airbus E-Fan electric aircraft, a comparison of the obtained optimal cruising speed at different values of C_I with the manufacturer's technical data showed that the proposed optimal solution yields realistic values for the cruising speed and maximum endurance.

5.2 Extensions

Several extensions to this work can be proposed for future research, namely:

- Find optimal solutions for the true airpseed and rates of climb and descent during climb and descent phases of flight. An important aspect is to ensure that the transitions between different flight segments are smooth.
- Consider a dynamic battery model proposed in [14] and obtain optimal solutions for electric

aircraft using nonlinear programming to validate assumptions made in the model.

- Take into consideration wind and turbulence effects.

- Explicitly account for state and input constraints in the mathematical formulation of the optimal control problem. For example, as it was shown in Chapter 4, the optimal speed for maximum range or maximum endurance of light-weight all-electric aircraft may be below its stall speed, and the constraint is not checked for until after the optimal solution is obtained. The same applies to turbofan aircraft where high C_I may lead to cruising at speeds above the drag divergence Mach number or those recommended by the manufacturer. The constraints must be explicitly incorporated in the optimal control problem.

- Extend the results obtained in Chapter 4 to the case of hybrid electric and hydrogen-powered aircraft.

Bibliography

[1] (2016) ATAG Facts & Figures. [Online]. Available: http://www.atag.org/facts-and-figures.html

[2] (2016) Airbus Global Market Forecast 2016-2035. [Online]. Available: http://www.airbusgroup.com/int/en/corporate-social-responsibility/airbus-e-fan-the-future-of-electric-aircraft.html

[3] (2017) Airbus E-Fan. The future of electric aircraft. [Online]. Available: http://www.airbusgroup.com/int/en/corporate-social-responsibility/airbus-e-fan-the-future-of-electric-aircraft.html

[4] J. Harrington, M. Kamlet, and K. Barnstorff. (2016) NASA Electric Research Plane Gets X Number, New Name. [Online]. Available: https://www.nasa.gov/press-release/nasa-electric-research-plane-gets-x-number-new-name

[5] M. Hepperle, "Electric flight – potential and limitations," in *NATO Science and Technology Organization. Meeting Proceedings*, 2012.

[6] S. Miller, "Contribution of flight systems to performance-based navigation," *Aero Magazine*, no. 34, pp. 21–28, 2009.

[7] A. Miele, *A survey of the problem of optimizing flight paths of aircraft and missiles*, 1st ed. Berkeley and Los Angeles: University of California Press, 1963, ch. 1, pp. 3–32.

[8] J. Sorensen, S. Morello, and H. Erzberger, "Application of trajectory optimization principles

to minimize aircraft operating costs," in *Proceedings of the 18th IEEE Conference on Decision and Control including the Symposium on Adaptive Processes*, 1979, pp. 415–421.

[9] J. Burrows, "Fuel-optimal aircraft trajectories with fixed arrival times," *Journal of Guidance, Control, and Dynamics*, vol. 6, no. 1, pp. 14–19, 1983.

[10] D. Pargett and M. Ardema, "Flight path optimization at constant altitude," *Journal of Guidance, Control, and Dynamics*, vol. 30, no. 4, pp. 1197–1201, 2007.

[11] A. Franco and D. Rivas, "Minimum-cost cruise at constant altitude of commercial aircraft including wind effects," *Journal of Guidance, Control, and Dynamics*, vol. 34, no. 4, pp. 1253–1260, 2011.

[12] R. Patrón and R. Botez, "Flight trajectory optimization through genetic algorithms for lateral and vertical integrated navigation," *Journal of Aerospace Information Systems*, vol. 12, no. 8, pp. 533–544, 2015.

[13] J. Villaroel and L. Rodrigues, "Optimal control framework for the cruise economy mode of flight management systems," *Journal of Guidance, Control, and Dynamics*, vol. 39, no. 5, pp. 1022–1033, 2016.

[14] O. Tremblay and L.-A. Dessaint, "Expiremental validation of a battery dynamic model for EV applications," *World Electric Vehicle Journal*, vol. 3, pp. 289–298, 2009.

[15] F. Morbidi, R. Cano, and D. Lara, "Minimum-energy path generation for a quadrotor UAV," in *Proceedings of the IEEE International Conference on Robotics and Automation*, 2016, pp. 1492–1498.

[16] A. Cândido, R. Galvão, and T. Yoneyama, "Control and energy management for quadrotor," in *Proceedings of the UKACC International Conference on Control*, 2014, pp. 343–348.

[17] R. Ritz, M. Hehn, S. Lupashin, and R. D'Andrea, "Quadrocopter performance benchmarking using optimal control," in *Proceedings of the IEEE/RSJ International Conference on Intelligent Robots and Systems*, 2011, pp. 5179–5186.

[18] L. W. Traub, "Range and endurance estimates for battery-powered aircraft," *Journal of Aircraft*, vol. 48, no. 2, pp. 703–707, 2011.

[19] T. Donateo, A. Ficarella, L. Spedicato, A. Arista, and M. Ferraro, "A new approach to calculating endurance in electric flight and comparing fuel cells and batteries," *Applied Energy*, vol. 187, pp. 807–819, 2017.

[20] T. Donateo and A. Ficarella, "Designing a hybrid electric powertrain for an unmanned aircraft with a commercial optimization software," *SAE International Journal of Aerospace*, vol. 10, pp. 807–819, 2017.

[21] J. D. Anderson, *Aircraft performance and design*, 1st ed. New York: McGraw-Hill, 1999.

[22] A. F. El-Sayed, *Fundamentals of Aircraft and Rocket Propulsion*, 1st ed. London: Springer, 2016.

[23] D. Doerffel and S. Sharkh, "A critical review of using the Peukert equation for determining the remaining capacity of lead-acid and lithium-ion batteries," *Journal of Power Sources*, vol. 155, pp. 395–400, 2006.

[24] L. Pontryagin, V. Boltyanskii, R. Gamkrelidze, and E. Mishchenko, *The Mathematical Theory of Optimal Processes*, 4th ed. Moscow: Nauka, 1983.

[25] D. Liberzon, *Calculus of variations and optimal control theory: A concise introduction*. Princeton University Press, 2012.

[26] M. Munir, H. Sali, and M. Ibtihal, "An efficient algorithm for computing the roots of general quadratic, cubic and quartic equations," *International Journal Of Mathematical Education In Science And Technology*, vol. 45, no. 7, pp. 1095–1103, 2014.

[27] M. Abramowitz and I. Stegun, *Handbook of Mathematical Functions: with Formulas, Graphs, and Mathematical Tables*. New York: Dover, 1972.

[28] H. Zoladek, "The topological proof of Abel-Ruffini theorem," *Journal of the Juliusz Schauder Center*, vol. 16, pp. 253–265, 2000.

[29] (2015) History is made, and the future of electric aircraft is opened with E-Fans English Channel crossing. [Online]. Available: http://www.airbusgroup.com/int/en/corporate-social-responsibility/latest-news/History-is-made--and-the-future-of-electric-aircraft-is-opened-with-E-Fan-s-English-Channel-crossing.html

[30] E. Joubert, D. Chapuis, D. Esteyne, J.-C. Lambert, O. Siri, and D. Müller-Wiesner, "The E-Fan all electrical aircraft demonstrator and its industrialization," in *Proceedings of the 30th Congress of the International Council of the Aeronautical Sciences*, 2016.

[31] J. Roskam and C.-T. E. Lan, *Airplane Aerodynamics and Performance*, 5th ed. DARcorporation, 2016.